

Key Points:

- The Lizard ophiolite formed above a subduction zone in the Rheic-Rhenohercynian Ocean around $386.80 \pm 0.25/0.31/0.52$ Ma
- The Landewednack Amphibolites, epidote-amphibolites and Old Lizard Head Series represent the inverted metamorphic sole of the ophiolite
- The metamorphic sole was subducted to conditions of 10 ± 2 kbar, with incipient cooling of partial melts at $395.08 \pm 0.14/0.22/0.47$ Ma

Supporting Information:

Supporting Information may be found in the online version of this article.

Correspondence to:

T. C. Mackay-Champion,
tobermory.mackay-champion@univ.ox.
ac.uk

Citation:




Mackay-Champion, T. C., Searle, M. P., Tapster, S., Roberts, N. M. W., Shail, R. K., Palin, R. M., et al. (2024). Magmatic, metamorphic and structural history of the Variscan Lizard ophiolite and metamorphic sole, Cornwall, UK. *Tectonics*, 43, e2023TC008187. <https://doi.org/10.1029/2023TC008187>

Received 17 NOV 2023

Accepted 23 FEB 2024

© Wiley Periodicals LLC. The Authors. This is an open access article under the terms of the [Creative Commons Attribution License](#), which permits use, distribution and reproduction in any medium, provided the original work is properly cited.

Magmatic, Metamorphic and Structural History of the Variscan Lizard Ophiolite and Metamorphic Sole, Cornwall, UK

Tobermory C. Mackay-Champion¹ , Michael P. Searle^{1,2,3} , Simon Tapster⁴, Nick M. W. Roberts⁴, Robin K. Shail² , Richard M. Palin¹, George H. Willment¹, and Josh T. Evans¹

¹Department of Earth Sciences, University of Oxford, Oxford, UK, ²Camborne School of Mines, Department of Earth and Environmental Science, University of Exeter, Cornwall, UK, ³Oxford University Museum of Natural History, Oxford, UK, ⁴Geochronology and Tracers Facility, British Geological Survey, Nottingham, UK

Abstract The Lizard ophiolite, Cornwall, South-West England, is the largest and best-preserved ophiolite within the Variscan orogenic belt. It forms part of the Rheic-Rhenohercynian suture zone, and was obducted northwestward onto the passive continental margin of Avalonia (Laurussia) during the Middle Devonian. It comprises an almost complete thrust slice of oceanic crust with sheeted dykes, gabbros, Moho transition sequence, and upper-mantle peridotites, underlain by a metamorphic sole. Despite the importance of the Lizard ophiolite in understanding Variscan tectonics, the origin and age of the Lizard ophiolite are debated. We present new field observations, structural maps and cross-sections of the Lizard ophiolite from extensive re-mapping, integrated with U–Pb geochronology, petrology, thermobarometry, and whole rock geochemistry. We report new U–Pb zircon (CA-ID-TIMS and LA-ICPMS) ages of $386.80 \pm 0.25/0.31/0.52$ Ma (Givetian) from a plagiogranite dyke intruding the Crousa Gabbros at Porthoustock, and $395.08 \pm 0.14/0.22/0.47$ Ma (Emsian) from partial melts of the metamorphic sole Landewednack Amphibolites at Mullion Cove. These ages, respectively, precisely date the formation of the Lizard ophiolite oceanic crust, and the age of cooling post peak-metamorphism of the sole. Petrological modeling on the Landewednack Amphibolites suggests peak metamorphic conditions of 10 ± 2 kbar and $600 \pm 75^\circ\text{C}$. We demonstrate that the Lizard ophiolite formed as a supra-subduction zone ophiolite overlying an inverted metamorphic sole, and we combine our observations and data into a new geodynamic model for the formation and obduction of the ophiolite. The current data supports an induced subduction initiation model.

1. Introduction

Ophiolites are allochthonous slices of oceanic crust and upper mantle emplaced onto continental margins during the initial stages of orogenesis (Coleman, 1971; Dilek & Furnes, 2014). They occur either as obducted thrust sheets emplaced large distances (>100 km) over previously passive continental margin sedimentary rocks, or as highly dismembered sequences which, together with relict oceanic rocks, define suture zones (Dilek & Furnes, 2014).

Originally interpreted as a high-temperature intrusion with a wide granulite–amphibolite facies metamorphic aureole (Green, 1964a, 1964b), the Lizard complex of Cornwall, South-West England (Figure 1), is now widely accepted as an obducted ophiolite, thrust toward the NNW onto the previously passive continental margin of Avalonia during the initial stages of the Variscan orogeny (Bromley, 1976; Holder & Leveridge, 1986; Kirby, 1979; Roberts et al., 1993; Shail & Leveridge, 2009; Strong et al., 1975; Styles & Kirby, 1980). It is one of the largest and best-preserved ophiolites of the Variscan orogenic belt, and therefore provides critical information on the early stages of the Variscan orogeny. The Lizard ophiolite also plays an important role in our understanding of the tectonic evolution of SW England and in particular, the geodynamics of Cornwall prior to the emplacement of the Sn–W–Cu-mineralized post-orogenic Cornubian batholith during the Permian. Despite this, no detailed tectonic model has been put forward for the formation and obduction of the Lizard ophiolite. Previous geochronological and structural constraints on units such as the Kennack Gneiss, a peraluminous felsic orthogneiss intruding into the metamorphic sole, appear to conflict, and there has been limited work on the pressure–temperature conditions and geodynamic evolution of the metamorphic sole. We identified four outstanding questions to examine in this study: (a) the pressure and temperature conditions experienced by the

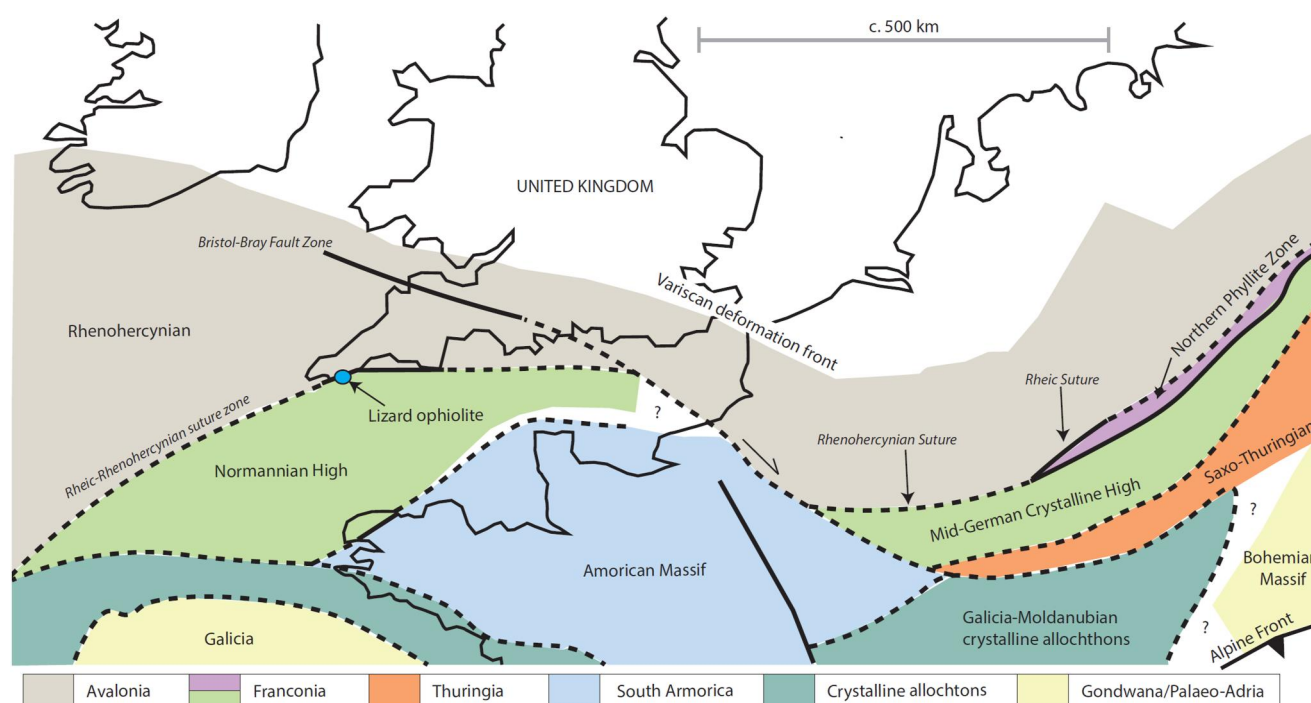


Figure 1. Simplified tectonic map of Europe, after Franke et al. (2017).

metamorphic sole, (b) the age of the Lizard ophiolite, (c) the age of the metamorphic sole and, (d) the geochemical similarities or differences between the metamorphic sole and the mafic rocks of the ophiolite.

Here, we present results from extensive re-mapping of the ophiolite complex and underlying metamorphic rock units around the Lizard peninsula, with a particular focus on the structural relationships between the ophiolite and the metamorphic sole. These new data are integrated with whole-rock geochemistry, new pressure–temperature modeling of the metamorphic units, and two new high-precision U–Pb zircon ages (plagiogranite and sole amphibolite). We propose a new tectonic model for the Lizard, which provides important constraints on the early stages of the Variscan orogeny.

2. Geological Setting

The SW England study area is part of the Rhenohercynian Zone of the European Variscan orogen (Figure 1). The Variscan Orogeny led to the formation of Pangaea after the closure of the Rheic Ocean (e.g., Murphy et al., 2006; Nance & Linnemann, 2008). The detailed timing of Rheic ocean closure, and the nature and polarity of its associated subduction zones and suture(s) are not fully constrained and a “two-stage” collision model for the consolidation of Pangaea is increasingly recognized (e.g., Arenas et al., 2014). The Rhenohercynian Zone represents either a marginal ocean basin north of the Rheic Ocean during the Devonian, or a successor Rhenohercynian Ocean following the latest Silurian–earliest Devonian closure of the Rheic Ocean (e.g., Alexander et al., 2019; Eckelmann et al., 2014; Franke, 2000, 2024; Franke et al., 2017; Shail & Leveridge, 2009). Distinct expressions of the Rheic and Rhenohercynian sutures have been inferred, in the Spessart Mountains (Germany), but the two sutures are generally shown as coincident and described as the Rheic-Rhenohercynian suture zone (Franke, 2024; Franke et al., 2017). This suture, which is approximately 8 km wide, is imaged cutting the whole crust on reflection seismic profiles across the English Channel (Alexander et al., 2019; BIRPS and ECORS, 1986; Klemperer & Hobbs, 1992; Le Gall, 1990). The suture zone separates a lower plate (SW England) from the upper plate Normannian High/Mid-German Crystalline Rise, that formed the southern active margin of this ocean basin (Franke, 2024; Franke et al., 2017; Holder & Leveridge, 1986). The Lizard ophiolite (Figure 2) represents the most complete ophiolite of the Rheic-Rhenohercynian suture zone, and therefore provides critical information on the geodynamics and timing of the early stages of the Variscan orogeny.

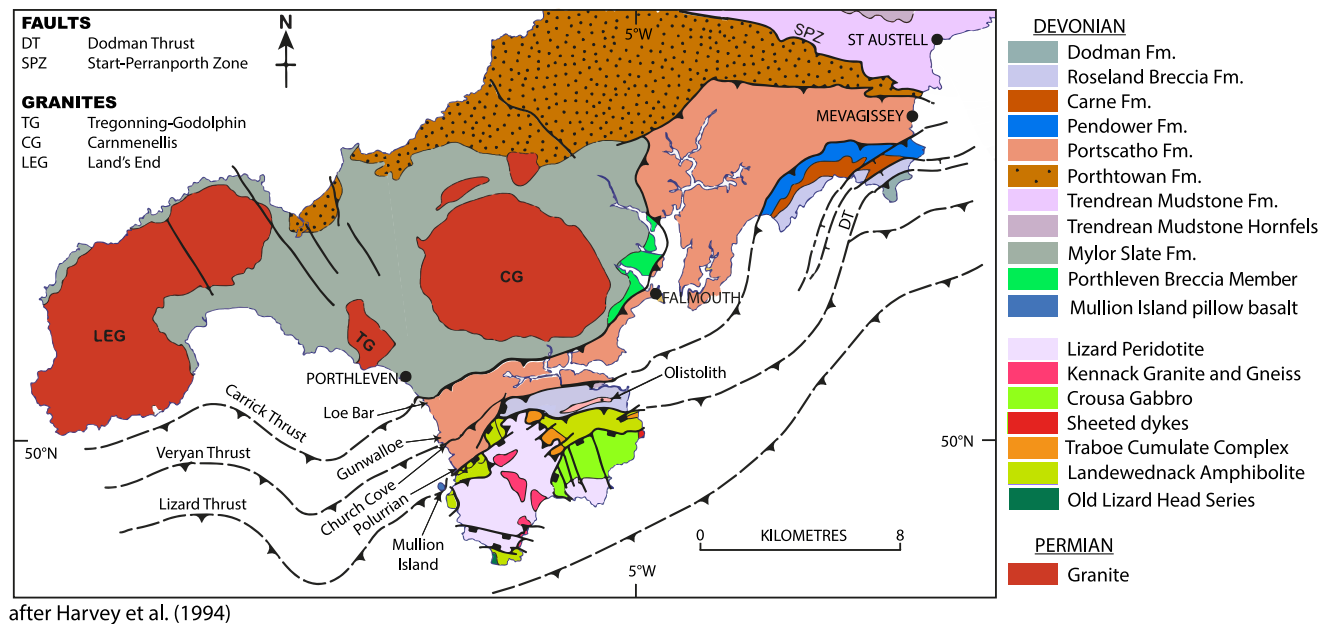


Figure 2. Geological map of south-west Cornwall, after Harvey et al. (1994).

3. Ophiolites and Subduction Dynamics

The ophiolite concept dates from the Penrose meeting of 1972 (Anonymous, 1972), when the succession of oceanic pillow lavas, sheeted dykes, lower crust gabbros, and upper mantle peridotites observed in many mountain belts of the world was compared to the geological and geophysical structure of the present-day oceans. Since then, the ophiolite concept has been extensively applied and tested in regions where type sections are well preserved, such as the Troodos Massif, Cyprus and the Semail ophiolite in Oman (e.g., Searle & Cox, 1999a; Varga & Moores, 1985). These allochthonous slices of oceanic lithosphere are exposed along some convergent continental margins, following the processes of obduction and emplacement. Ophiolite obduction is contemporaneous with the subduction of the passive continental margin beneath the ophiolite, leading eventually to final ophiolite emplacement (Coleman, 1971). A strong continental basement is required for ophiolite emplacement (Duretz et al., 2016). Ophiolites are often thrust over a thin sequence of metamorphic rocks showing inverted metamorphic isograds, known as the metamorphic sole (Jamieson, 1980; Searle & Malpas, 1980; Wakabayashi & Dilek, 2000). These rocks generally range from amphibolites, with or without garnet and clinopyroxene at the higher structural levels, through to greenschist facies metasediments at the base. Metamorphic soles form from the uppermost crust of the subducting slab and are accreted along the base of the ophiolite during early oceanic subduction (e.g., Ambrose et al., 2021; Searle & Cox, 2002; Searle & Malpas, 1980; Soret et al., 2017).

There are two broad categories of ophiolites: subduction-unrelated and subduction-related (Dilek & Furnes, 2014). Subduction-unrelated ophiolites are those which formed at spreading ridges without the influence of subduction processes and include Mid-Ocean Ridge (MOR) ophiolites. In MOR ophiolites, the metamorphic sole forms after spreading ceases (e.g., Wakabayashi & Dilek, 2000). Consequently, the age of metamorphism of the metamorphic sole should be synchronous with, or younger than the age of ophiolite rocks (e.g., plagiogranites, gabbros). For example, the metamorphic sole of the MOR Palawan ophiolite in the Philippines, is ~1 Myr younger than the overlying ophiolite (Keenan et al., 2016). However, most ophiolites appear to have formed above nascent subduction zones (e.g., Pearce et al., 1984). These ophiolites belong to the subduction-related category and are known as Supra-Subduction Zone (SSZ) ophiolites. The onset of oceanic subduction is critical to the interpretation of SSZ ophiolites. There are currently two end-member models for the process of subduction initiation: Induced Subduction Initiation (ISI) and Spontaneous Subduction Initiation (SSI) (Stern, 2004). ISI involves the forced underthrusting of oceanic lithosphere below adjacent oceanic lithosphere as the result of regional plate dynamics (Gurnis, et al., 2004; Hall et al., 2003). Underthrusting was likely initiated at pre-existing weak structures within the lithosphere. In this model, upper plate spreading only begins once subduction becomes self-sustaining and the hinge of the subduction zone retreats (i.e., the metamorphic sole

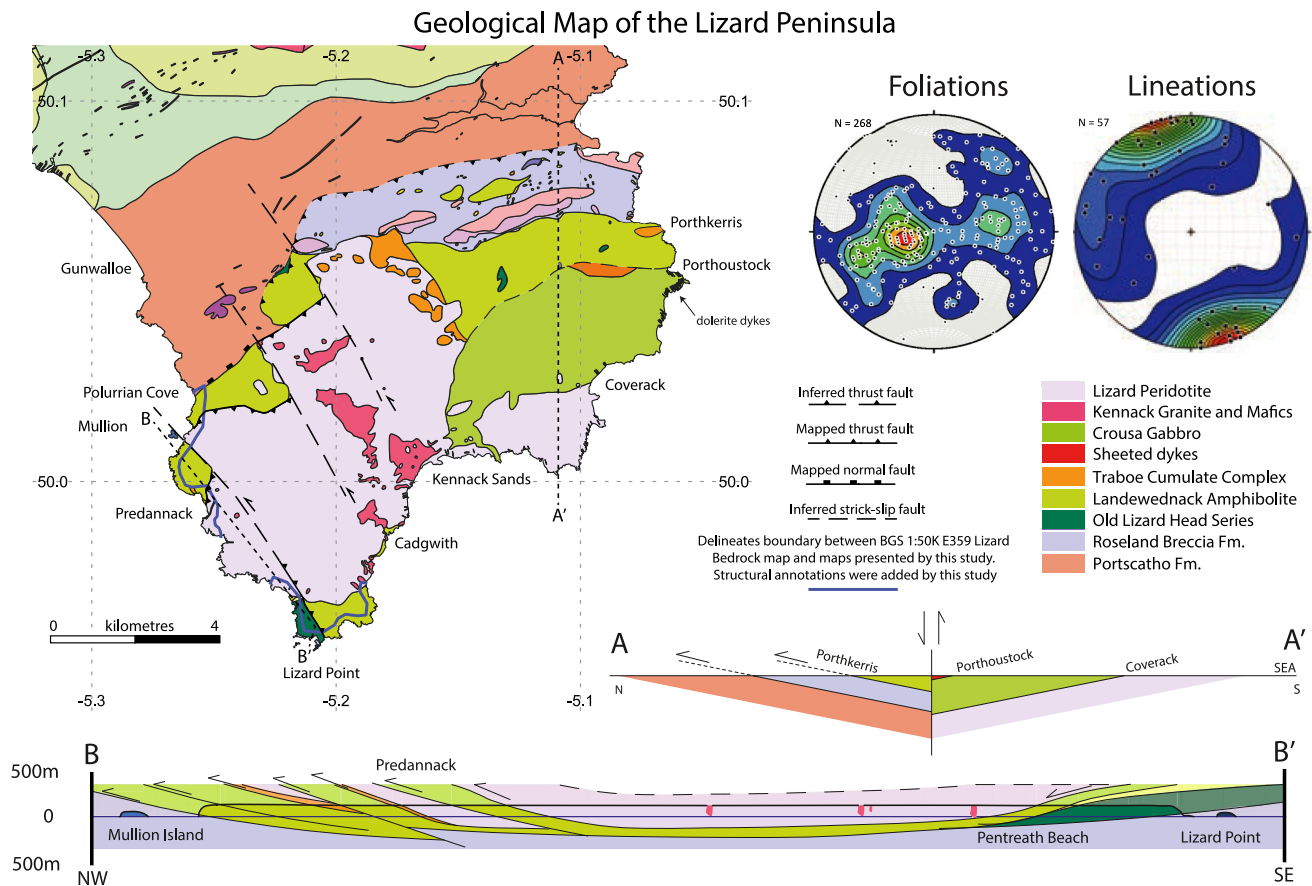


Figure 3. Regional map of the Lizard ophiolite, with accompanying cross-sections and stereonets. The blue lines on the map delineate the boundary between BGS 1:50K E359 Lizard Bedrock map and new maps presented by this study. The structural annotations were added by this study. The BGS 1:50K E359 Lizard Bedrock map is reproduced with the permission of the British Geological Survey © UKRI 2022. All Rights Reserved.

experienced metamorphism prior to SSZ ophiolite formation). SSI results from spontaneous lithospheric “collapse” and subsequent subduction of oceanic crust due to gravitation instability at zones of weakness, such as oceanic transform faults (Stern, 2004). The spontaneous sinking of the downgoing slab causes the hinge of the subduction zone to retreat, driving concurrent supra-subduction zone spreading in the upper plate (i.e., the metamorphic sole experienced metamorphism at the same time as ophiolite formation). Consequently, the time lag between the metamorphism of the metamorphic sole and the formation of the ophiolite can be used to determine whether SSI or ISI is most appropriate for a given ophiolite (e.g., Guilmette et al., 2018; Soret et al., 2022).

The Lizard ophiolite has previously been categorized as a mid-ocean ridge ophiolite, largely based on the MORB characteristics of gabbros and dolerite dykes on the Lizard peninsula (e.g., Bromley, 1976; Leveridge & Shail, 2011). However, ophiolite rocks can display MORB geochemistry despite forming in a subduction zone environment (e.g., the Geotimes volcanic unit of the Semail ophiolite, Pearce et al., 1984). Ishizuka et al. (2011) estimated that the transition from forearc basalt magmatism with a MORB-like geochemistry to boninitic magmatism in the Izu-Bonin-Mariana forearc spreading center lasted around 7 Myr. Therefore, the geochemical characteristics of the Crousa Gabbro unit and associated dolerite dykes alone are not adequate to distinguish between a MOR or SSZ model of formation. This study re-examines whether the Lizard ophiolite formed above a subduction zone and if so, was subduction initiation spontaneous or induced by regional tectonics.

4. Lizard Ophiolite: Field Relations and Petrography

In this section, we combine previously published data with our own field observations and analysis to provide a new synthesis and interpretation of the geology of the Lizard peninsula. We carried out structural mapping of

selected areas of the Lizard Peninsula, SW England at 1:10,000 and outcrop scale. Key areas were mapped (Figure 4) and then combined with previous maps published by the British Geological Survey (BGS 1:50K E359 Lizard Bedrock map) to obtain a complete framework of the structure of the Lizard Peninsula. These new geological maps, with an accompanying tectonostratigraphic column, cross-sections and stereograms, are presented in Figures 3–5. The BGS color scheme has been used throughout this study. For clarity, structural measurements have been omitted from the maps but may be found in Supporting Information S1. The new mapping efforts are distinguished from the BGS using thick blue lines (e.g., Figure 4). The new field observations have allowed us to identify, re-interpret, and characterize the key tectonostratigraphic units within the Lizard Ophiolite. The best profile through the entire ophiolite sequence extends along the east coast of the Lizard from Cadgwith through Coverack to Porthkerris, along which mantle peridotites, the crust-mantle boundary, and crustal gabbros and sheeted dykes are almost continuously exposed (Figure 3).

4.1. Mantle Sequence Peridotites

Upper mantle rocks exposed in the Lizard ophiolite include spinel lherzolite (ol + opx + cpx + sp), and depleted mantle harzburgite (ol + opx) and dunite (olivine) all of which are strongly serpentinized. The Lizard Thrust is the basal contact of the mantle sequence with the underlying Landewednack Amphibolites and is particularly well exposed at a small cove south of Mullion (Figure 6a). Fabrics are defined by aligned olivine, orthopyroxene, epidote and secondary hornblende, with prominent bastite pseudomorphs after enstatite. Hydrothermal veins of serpentine (lizardite, antigorite, chrysotile), talc and asbestos veins show a classic chess-board pattern (Figure 5f). Along the base of the ophiolite mantle sequence a strong mylonitic fabric, parallel to the Lizard Thrust, has been imposed on the lherzolite. At Mullion Cove, the contact and the basal fabric in the peridotites strikes approximately N-S and dips steeply ESE. Along the east coast of the Lizard peninsula, the basal contact of the peridotites undulates sub-horizontally and has been cut by later faulting. It is well exposed north (Kiltdown Point), and south (The Balk) of Cadgwith, and along the cliffs southwest of Kennack Sands (Cook et al., 2002). At all these localities, the fabric in the base of the mantle sequence have been cut by intrusions of felsic Kennack granitic gneiss (Sandeman et al., 2000).

4.2. Moho Transition Zone, Coverack

The oceanic crust–upper mantle boundary is defined as the Moho transition zone (MTZ) and is particularly well exposed at Coverack cove (Roberts et al., 1993). The Moho is rarely a planar feature but is instead a zone up to 1–2 km thick comprising layered ultramafic peridotites and gabbros intruded by troctolite (ol + pl) dykes or sills, and a set of NW-SE aligned dolerite dykes. Small-scale gabbroic veins within peridotites are interpreted as the products of in situ melting in the uppermost mantle. These melts become progressively thicker up-section in the MTZ where several gabbro sills intrude the peridotite. Gabbros are composed of olivine altered to serpentine, clinopyroxene altered to hornblende, and saussuritised plagioclase. The MTZ crops out along the length of Coverack Beach with massive coarse-grained gabbros appearing at the northern end of the beach.

4.3. Lower Crust Gabbros, Coverack

North of Coverack, lower crust gabbros show igneous layering interpreted as cumulus textures with small-scale olivine-rich bands passing structurally upward to more plagioclase-rich gabbros (Kirby, 1979). Olivine crystals accumulated by gravitational settling along the floor of each magma intrusion, with inter-cumulus poikilitic clinopyroxene and plagioclase. Dunite pods along the base of the gabbros probably represent the restitic depleted mantle from which tholeiitic magma has been extracted. A few doleritic dykes intrude the gabbro sequence and the uppermost part of the mantle. These plagioclase- and olivine phyric dykes are distinct from the plagioclase-phyric sheeted dyke complex exposed near Porthoustock (e.g., Roberts et al., 1993). There, the gabbros merge directly into the base of the sheeted dykes (Figures 5a and 5b), field relations typically seen in other better exposed ophiolites such as the Semail ophiolite (Oman) or the Troodos ophiolite (Cyprus).

4.4. Traboe Cumulate Sequence, Porthkerris

A sequence of cumulate gabbros exposed at Porthkerris on the east coast of the Lizard, and in patches along the west coast at Predannack, has previously been described as a separate unit—the Traboe cumulate sequence (Figures 3 and 4) (Green, 1964a). Green initially proposed that these rocks were high-temperature granulites in a

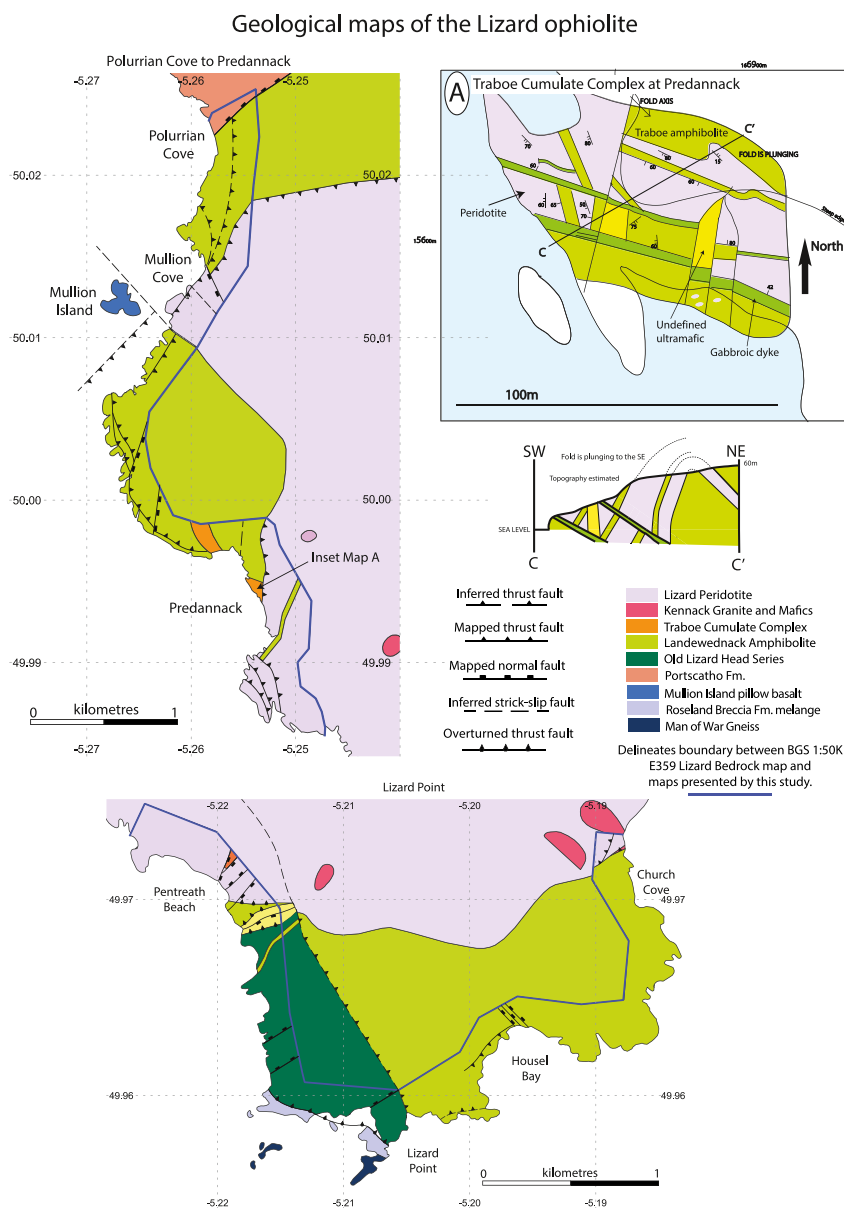


Figure 4. New geological maps of the Lizard ophiolite and underlying units. The blue lines on the map delineate the boundary between BGS 1:50K E359 Lizard Bedrock map and new maps presented by this study. The structural annotations were added by this study. The BGS 1:50K E359 Lizard Bedrock map is reproduced with the permission of the British Geological Survey © UKRI 2022. All Rights Reserved.

contact metamorphic aureole around the intrusive peridotite. The two-pyroxene Traboe gabbros have complex igneous textures such as igneous layering, cumulate textures, flow-banding, etc. (Leake & Styles, 1984). They contain orthopyroxene (hypersthene) + clinopyroxene (diopside, augite) + hornblende + plagioclase + ilmenite, and are occasionally interleaved with serpentinized peridotites. At Porthkerris, these two-pyroxene gabbros show igneous banding, overprinted by strong high-temperature ductile shear fabrics, and intruded by coarse-grained pegmatites (e.g., Gibbons & Thompson, 1991) (Figure 7a). Contacts of the Traboe cumulates are fault-bounded with Landewednack Amphibolites to the south, and melange units to the north at Porthallow. We suggest that the Traboe Cumulate sequence is part of the ophiolite sequence, following Styles and Kirby (1980) and Leake and Styles (1984). In the outcrops at Predannack (Figures 4 and 6b), peridotite is interlayered with amphibolite, both of which are intruded by dolerite dykes. These relations suggest that either faulting under the ocean floor or dyke intrusion juxtaposed hot peridotite with gabbro, causing metamorphism of the gabbro to

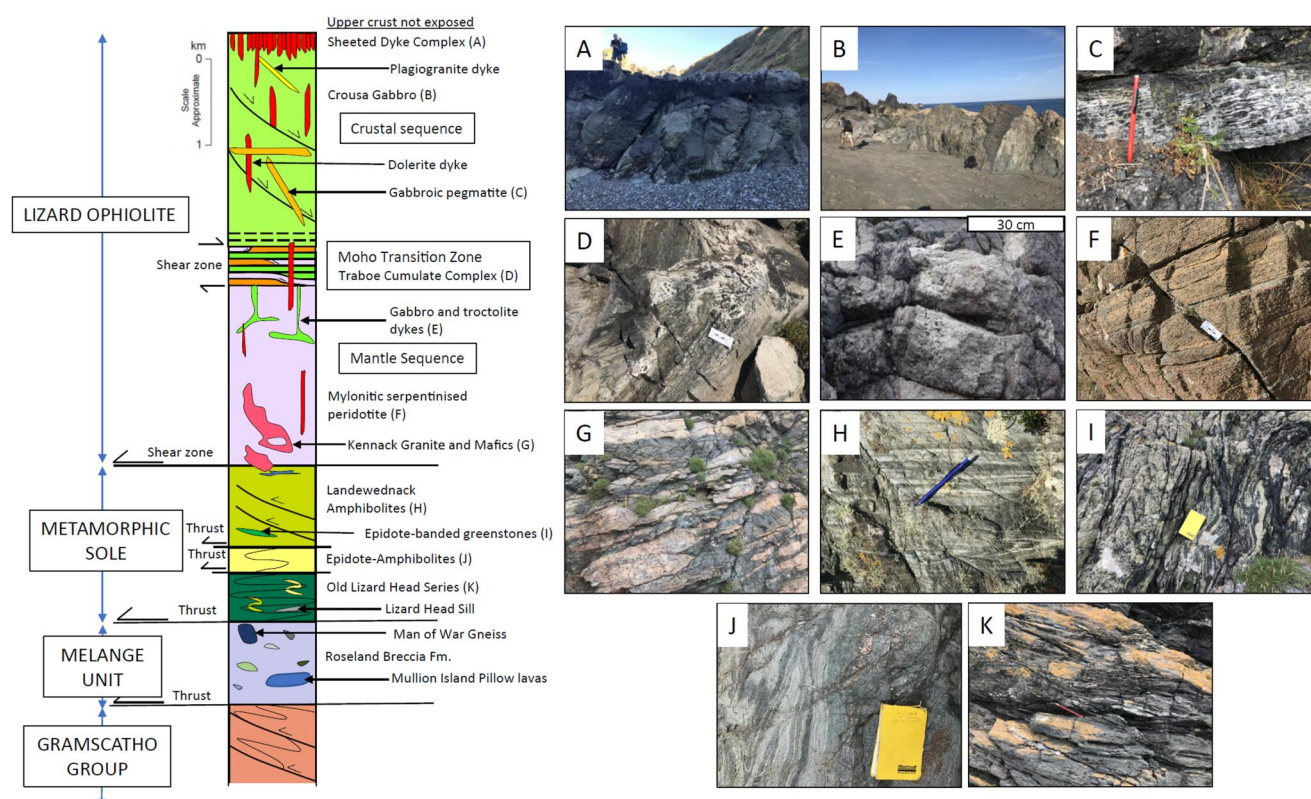


Figure 5. Tectonostratigraphic column for the Lizard ophiolite and underlying units.

amphibolite. The intrusion of the later dolerite dykes suggests that this occurred close to the spreading ridge. The outcrops at Predannack and Porthkerris both suggest that the Traboe sequence formed as a result of deformation of the ophiolite during spreading.

4.5. Carrick Luz Shear Zone

Amphibolite-facies, ductile shear zones cut through the gabbros and appear to sole in the MTZ. The mylonites trend NW-SE and have sub-horizontal mineral lineations in present-day orientation demonstrating a top-to-the-SE shearing of gabbro over the peridotite (Allerton & Macleod, 1998; Gibbons & Thompson, 1991). The best exposure of these low-angle normal shear zones crops out at Carrick Luz, east of Kennack Sands. These listric low-angle ductile shear zones are interpreted as extensional faults and are likely related to lower oceanic crustal extension along an oceanic ridge spreading center (Gibbons & Thompson, 1991). Some dolerite dykes are affected by the mylonitization, others cut across the mylonite fabric. The origin of these dolerite-basalt dykes cutting lower crust gabbros and even upper mantle peridotites remains speculative, but they do not appear to be connected spatially to the ophiolitic sheeted dyke complex at higher structural levels.

4.6. Plagiogranite Dykes, Porthoustock

Rare plagiogranite dykes are observed intruding the upper part of the ophiolite Crousa Gabbros at Porthoustock (Figure 7b) (e.g., Davies, 1984). These rocks are composed almost entirely of saussuritised plagioclase with minor prismatic hornblende, altered to sericite. Like other ophiolite plagiogranites, we interpret them as the final fractionated phase of the tholeiitic ophiolite melting sequence. Magma mingling and mixing textures between the plagiogranite dykes and the surrounding Crousa Gabbro suggest that they are approximately contemporaneous. The plagiogranite is composed of saussuritised plagioclase with minor quartz, chlorite, titanite and carbonate (Figure 8a). Some chlorite grains form in aggregates that may be pseudomorphs after a primary ferromagnesian mineral such as amphibole. This assemblage records pervasive post-crystallization hydrothermal alteration at greenschist-facies conditions.

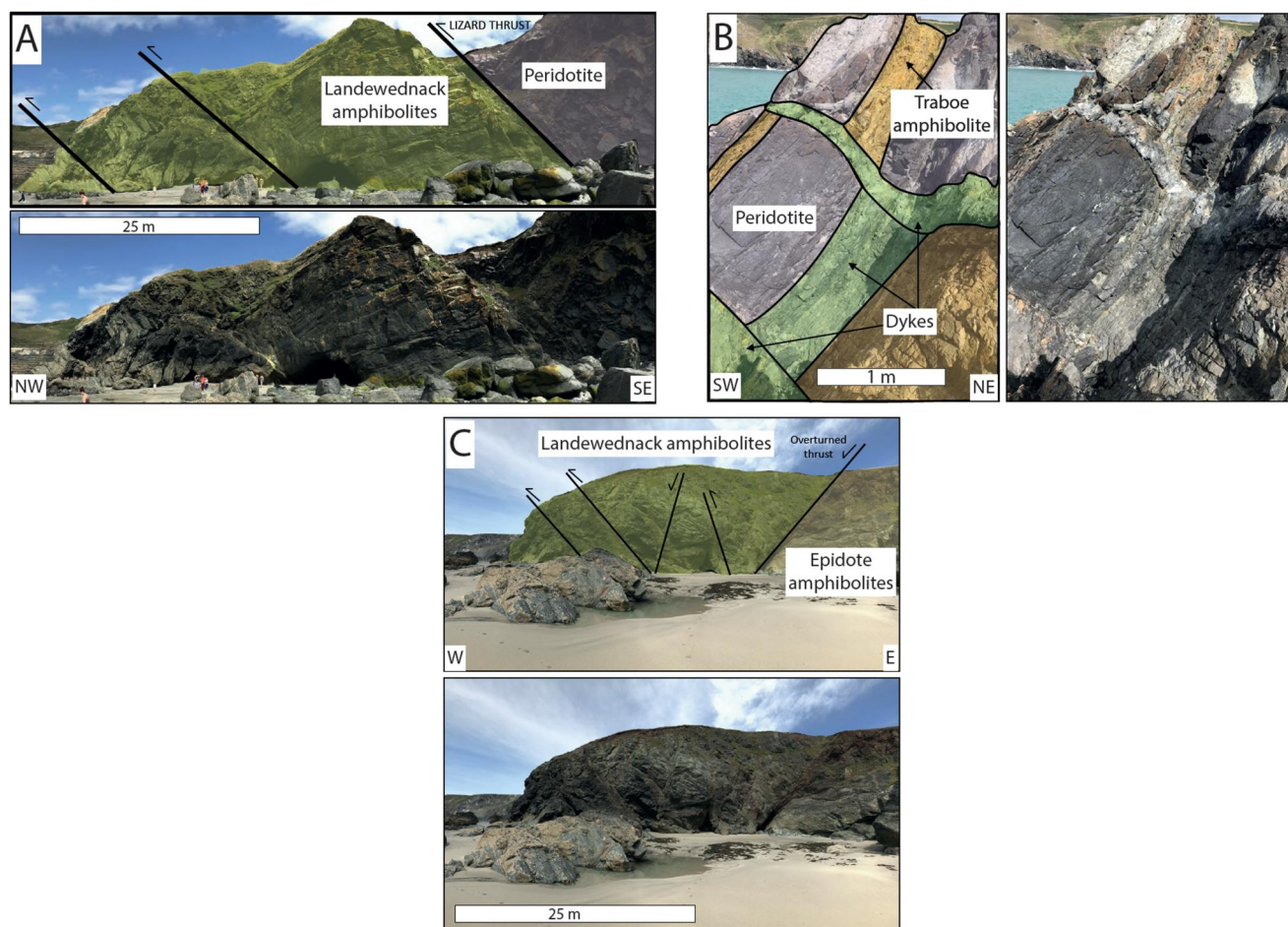


Figure 6. Field relationships in the Lizard Peninsula. (a) The Lizard Thrust at Mullion Cove, separating the overlying Lizard Peridotite from the Landewednack amphibolites of the metamorphic sole; (b) The Traboe Complex, Predannack; (c) An overturned thrust contact separating the higher-grade Landewednack amphibolites from the underlying, lower-grade epidote-amphibolites at Pentreath Beach. These units both belong to the metamorphic sole.

4.7. Sheeted Dykes, Porthoustock

The highest structural level of the Lizard ophiolite is represented by the sheeted dyke complex exposed at Porthoustock on the northeast coast of the Lizard peninsula (Figure 5a). These plagioclase-phyric dolerite dykes trend NW-SE and dip to the NE and are transitional with the underlying massive gabbros, and therefore are part of the main Lizard ophiolite sequence. The dykes have plagioclase phenocrysts in a groundmass of plagioclase, clinopyroxene altered to amphibole, and olivine with a tholeiitic MORB geochemical trend (Roberts et al., 1993). Pillow lavas and associated oceanic deep-sea sedimentary rocks are not exposed along this ophiolite section, having been eroded.

5. Metamorphic Sole: Field Relations and Petrography

A series of amphibolite-facies metamorphic rocks, the Landewednack amphibolites, are closely associated with the peridotites of the Lizard ophiolite (Cook, et al., 2002; Jones, 1997), and are interpreted as the disrupted parts of a sub-ophiolite metamorphic sole (e.g., Sandeman et al., 1995), similar to rocks mapped beneath other obducted ophiolites such as the Bay of Islands, Newfoundland (Williams & Smyth, 1973) and Oman (Searle & Malpas, 1980, 1982). Unlike both Newfoundland and Oman, no granulite facies minerals such as garnet or clinopyroxene have been recorded from the Landewednack amphibolites. Although many contacts have been overprinted by later faulting, the original thrust contact between the Landewednack amphibolites and the overlying Lizard peridotite can be clearly observed at Mullion Cove, where a 45° SE dipping thrust fault places highly sheared lherzolites over amphibolites of the metamorphic sole (Figure 6a). The original Lizard Thrust contact is

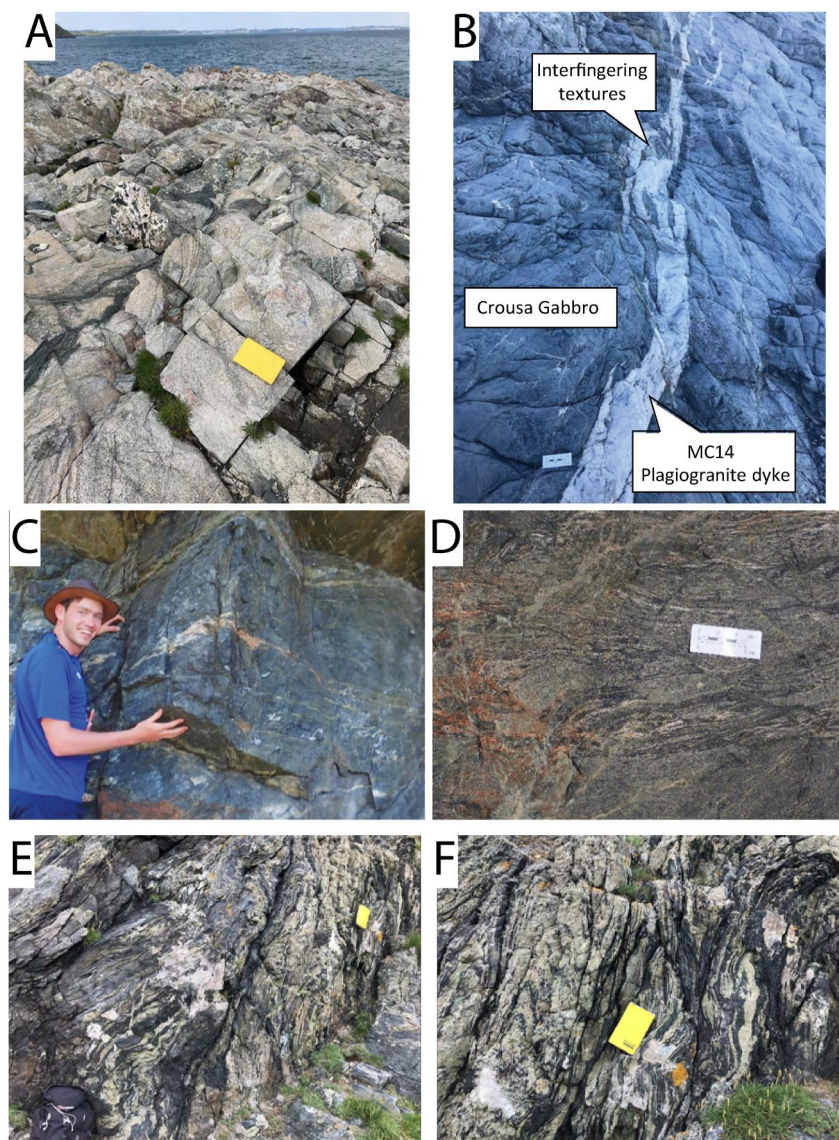


Figure 7. Outcrops from the Lizard Peninsula. (a) Deformed gabbro, Porthkerris; (b) Plagiogranite dyke, Porthoustock; (c) and (d) In situ partial melts from within the Landewednack amphibolites, Housel Bay; (e) and (f) Banded epidote-amphibolites, Housel Bay.

also well exposed at Kiltown Point near Cadgwith Cove (e.g., Cook et al., 2002; Sandeman et al., 1995), where small-scale in situ partial melting of the amphibolite is apparent up to 10 m below the peridotite contact (e.g., Figure 7c from Housel Cove). The Lizard Thrust contact undulates sub-horizontally from Cadgwith Cove to Kennack Sands along the east coast of the Lizard peninsula. The Landewednack amphibolites are fine to medium-grained and relatively uniform in mineralogy, characterized by amphibole (magnesian hornblende), plagioclase (andesine), minor quartz, ilmenite and titanite (Figure 8b). Several of the amphibole crystals preserve earlier amphiboles as inclusions within their cores (Figure 8c). Metamorphic clinopyroxene is interpreted to have been present but has been largely replaced by retrograde hornblende. Some samples are dominated by amphibole, whereas others are dominated by plagioclase. This variation likely reflects lithological heterogeneity within the mafic protolith and/or differences in the degrees of partial melting. The compositions of plagioclase and amphibole crystals in two samples of the Landewednack Amphibolites are shown in Figure 10 and will be discussed further in Section 6. Where present, mineral lineations and S-C fabrics suggest a top-to-NW or NNW sense of shear, consistent with NNW-directed obduction of the ophiolite onto the continental margin. A body of highly strained, banded epidote-amphibolites crops out amongst the Landewednack amphibolite on the eastern

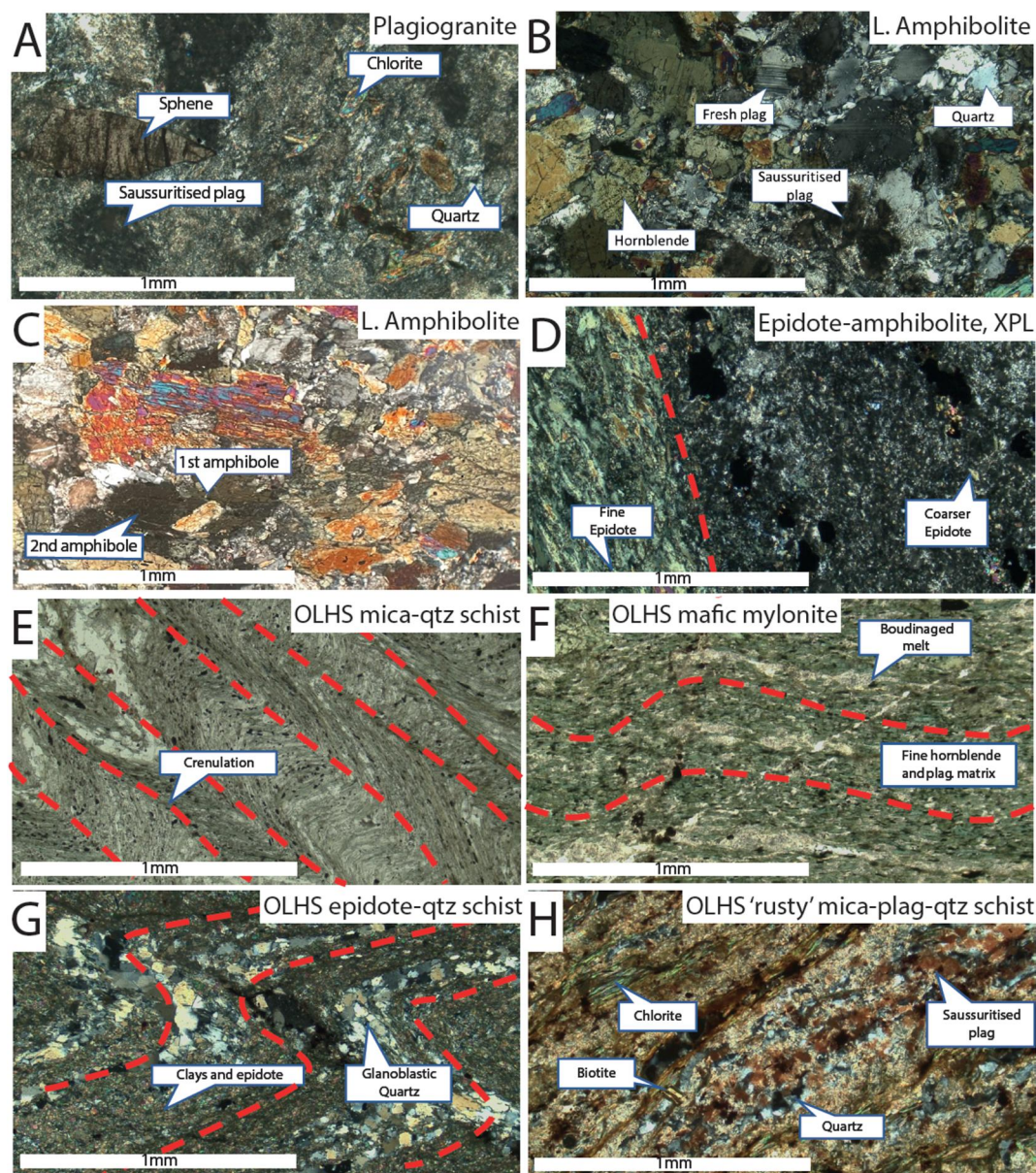


Figure 8. Photomicrographs from the Lizard ophiolite and underlying units. (a) Plagiogranite, Sample MC14; (b) Landwednack Amphibolite, Sample MC1; (c) Landwednack Amphibolite, Sample MC1; (d) Epidote-amphibolite, XPL; (e) Old Lizard Head mica-quartz schist; (f) Old Lizard Head Series mafic mylonite; (g) Old Lizard Head Series epidote-quartz schist; (h) Old Lizard Head Series mica-plagioclase-quartz schist.

side of Housel Bay. They exhibit banding on the centimeter to decimeter scale and are highly strained (Figures 7e and 7f). The body is not fault bounded, suggesting it represents lithological variation within the Landwednack Amphibolites. Based on similar examples in the Tauern Window, Eastern Alps (D. Waters, personal communications, 2021), it is possible that the epidote-rich layers of the banded amphibolite in the Lizard represent highly strained, metamorphosed pillow basalt structures.

Lower temperature epidote-bearing amphibolites have been identified structurally beneath the main amphibolites south of Pentreath beach (Figure 6c), suggesting a potential inverted metamorphic gradient below the peridotites. These lower temperature amphibolites are characterized by abundant epidote, alongside plagioclase and amphibole (Figure 8d). They appear to have formed from the same mafic protolith as the Landwednack

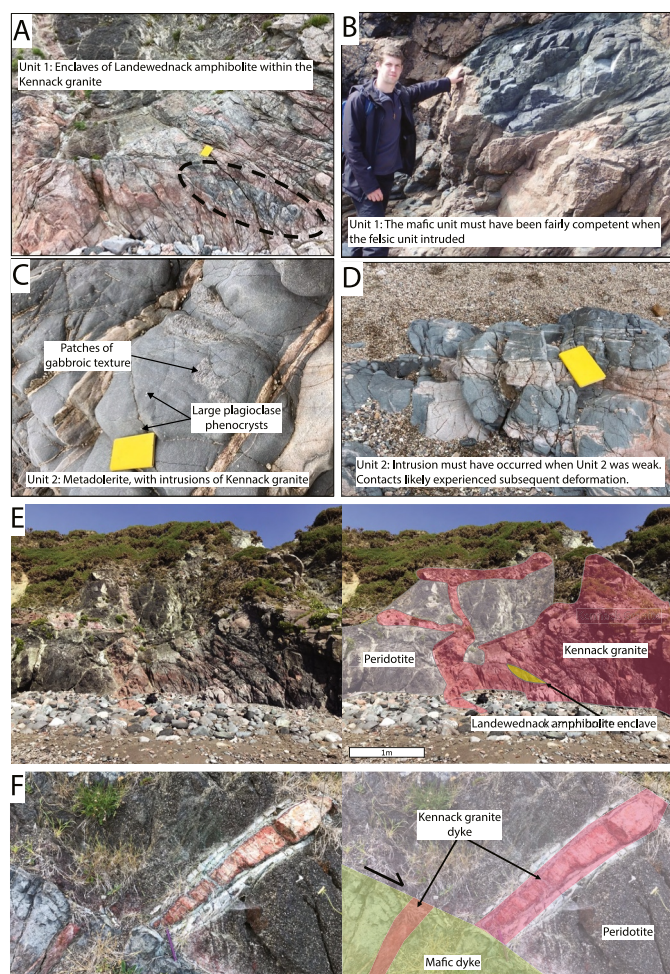


Figure 9. Field relationships of the Kennack Gneiss at Kennack Sands.

ange (Leveridge & Shail, 2011) structurally beneath the Lizard ophiolite, and may represent unmetamorphosed equivalents of the Landewednack amphibolites. The *mélange* formed during ophiolite obduction, during which much continental material would have been incorporated (e.g., Holder & Leveridge, 1986). Structurally beneath the *mélange* is a series of strongly folded and thrust units of Upper Devonian—Carboniferous sedimentary rocks of the Gramscatho Group (Shail & Leveridge, 2009).

6. Kennack Gneiss: Field Relations and Petrography

The Kennack Gneiss has previously been described as an interlayered sequence of mafic and felsic gneisses that intrudes the base of the Lizard ophiolite complex (Flett & Hill, 1946; Malpas & Langdon, 1987; Sandeman et al., 2000; Styles & Rundle, 1984; Teall, 1886). Although previous studies have labeled this unit a “gneiss,” the textures are largely magmatic in origin and therefore the term gneiss is perhaps misleading. For clarity, the original igneous names have been adopted here. The proportion of mafic to felsic components in the interlayered unit varies between outcrops. The felsic component ranges from granodiorite to peraluminous syenogranite, and contains K-feldspar in addition to plagioclase, quartz, and biotite. K-feldspar and quartz show intergrowth textures. These granitoids intrude the base of the peridotite at Kennack Sands, Kynance Cove, and Pentreath (Figures 9e and 9f). The abundance of potassium, up to 5.6 wt. % K_2O (Sandeman et al., 2000), and their field position suggests that the granites originated from melting of sedimentary rocks structurally beneath the ophiolite. This likely occurred during the later stages of obduction (Malpas & Langdon, 1987).

Three groups of mafic components were defined by Sandeman et al. (2000) on the basis of their petrographic characteristics. Group 1, the most abundant unit, is a hornblende-plagioclase schist with a micro-gabbroic to

Amphibolites but display a stronger foliation and more intense folding. The higher proportion of epidote compared to epidote-poor equivalents may represent a more oxidized protolith.

The Old Lizard Head Series is a sequence of highly deformed, upper greenschist facies pelitic schists and quartzites with a prominent felsic sheet known as the Lizard Head Sill (Figure 5k) (Sandeman et al., 1997). The pelitic and semi-pelitic schists comprise predominantly chlorite, muscovite, biotite, quartz, and feldspar, with minor garnet in some units. This assemblage suggests metamorphism at greenschist to lower amphibolite facies conditions, as expected of the structurally lower greenschist part of the metamorphic sole. Intense folding and crenulation cleavages are pervasively developed (Figure 8e). The incorporated mafic sheets of amphibolite and epidote-amphibolite comprise albitic plagioclase and magnesiohornblende, and display extensive ductile deformation, with folding, mylonitization and boudinage of melt layers (Figure 8f). Previously interpreted as metamorphic basement (Cook et al., 2002), we interpret the Old Lizard Head Series as sedimentary and volcanic rocks deposited on the continental shelf of Avalonia during the formation of the Lizard ophiolite. We include this sequence in the metamorphic sole given the structural position below the Landewednack amphibolites and below the Lizard peridotites.

At Lizard Point, the Old Lizard Head Series is in thrust contact with an underlying unit comprising deformed schists and the Man of War Gneiss (Figure 4) (Jones, 1994). The thrust fault has been overturned, with the Old Lizard Head Series thrust to the north-west over the underlying unit. The Man of War Gneiss is a body of medium-grained, gabbroic to tonalitic, meta-igneous rock which crops out as a series of outlying offshore rocks at Lizard Point and has been previously interpreted as metamorphic basement (Cook et al., 2002; Sandeman et al., 1997). We interpret the unit underlying the Old Lizard Head Series to be part of the Roseland Breccia Formation *mélange*: the deformed schists represent the highly deformed *mélange* matrix, and the Man of War Gneiss represents a coherent block within the *mélange*. The Mullion Island pillow basalts are also a coherent block within the *mélange*.

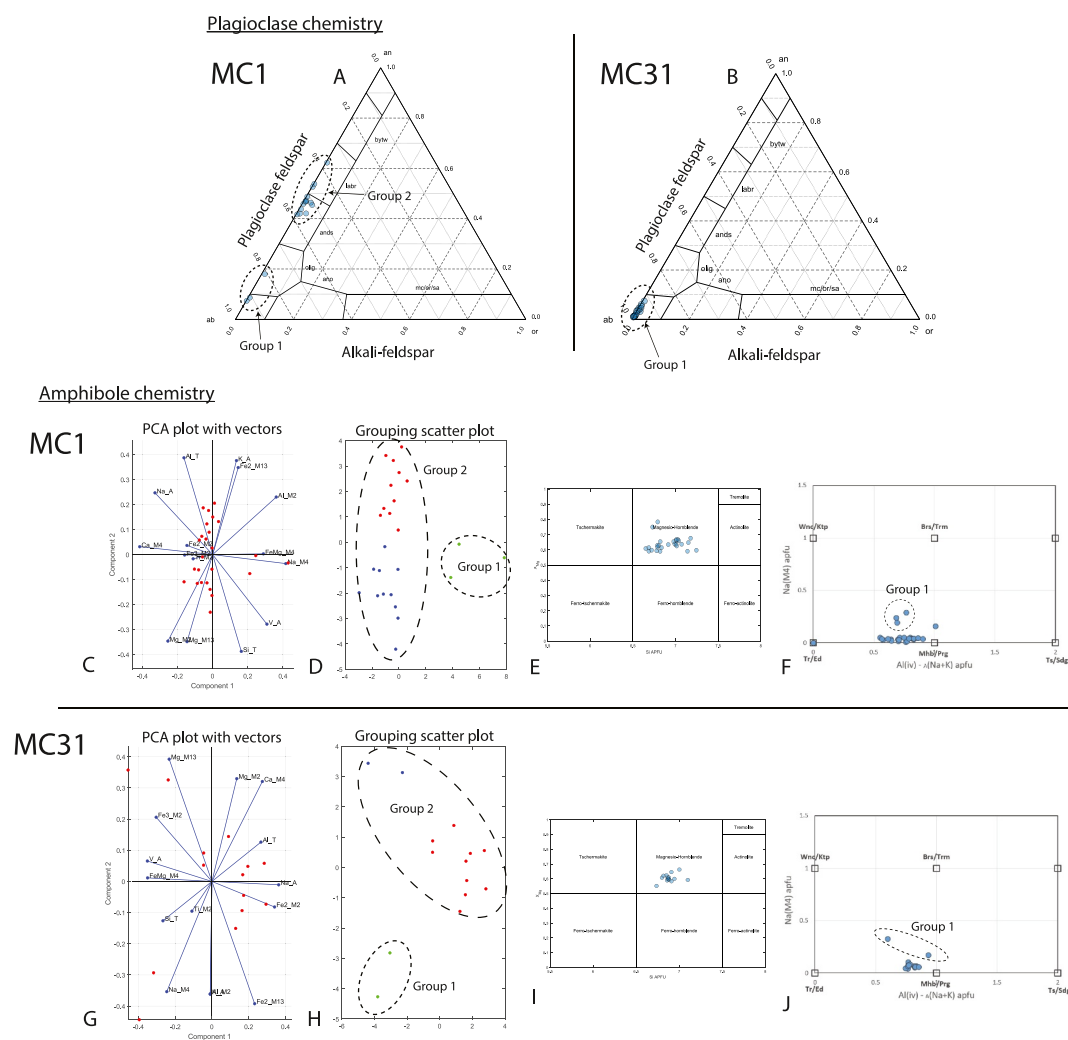


Figure 10. Mineral chemistry of the metamorphic sole. (a) Plagioclase compositions, Sample MC1. (b) Plagioclase compositions, Sample MC31. (c) and (d) Principal Component Analysis biplots of amphibole compositions, Sample MC1. (e) Amphibole compositions, Sample MC1 after Leake et al. (1997). (f) Amphibole compositions, Sample MC1 after Schumacher (2007). (g) and (h) Principal Component Analysis biplots of amphibole compositions, Sample MC31. (i) Amphibole compositions, Sample MC31 after Leake et al. (1997). (j) Amphibole compositions, Sample MC31 after Schumacher (2007).

gabbroic texture and occurs as elongate pods within the interlayered gneiss. Group 2a, the second most abundant unit, is a hornblende-plagioclase schist with crystal sizes <2.5 mm. Group 2b is a medium-grained biotite-amphibolite schist with large plagioclase “porphyroblasts,” and occurs as small, diffuse pods within the interlayered gneiss.

Given the complex textures within the interlayered units, it is difficult to ascertain whether the groups identified by Sandeman et al. (2000) do truly represent distinct lithologies, or whether they represent a continuum of interaction between the felsic and mafic lithologies and varying degrees of fractionation and metamorphism. The distinction between the groups based on immobile element geochemistry is challenging given the low number of samples. As such, we propose a new classification based purely on the field relationships between the felsic and mafic units: Unit 1 forms large and small-scale, coherent blocks of strongly to well foliated hornblende + plagioclase amphibolite within the granites (Figures 9a and 9b). These blocks have a similar mineralogy and fabric to the Landewednack amphibolites. We suggest that these rocks may represent xenoliths of metamorphic sole incorporated during intrusion of the granite into the base of the Lizard peridotite and metamorphic sole. The second mafic unit (Unit 2) is a metadolerite characterized by its complex relationships with the Kennack

Table 1

Bulk Composition of Samples MC1 and MC31 in wt% Oxide

| Sample | SiO ₂ (%) | TiO ₂ (%) | Al ₂ O ₃ (%) | FeO (%) | MnO (%) | MgO (%) | CaO (%) | Na ₂ O (%) | K ₂ O (%) | P ₂ O ₅ (%) | Cr ₂ O ₃ (%) | NiO (%) | SO ₃ (%) | LOI (%) | Sum (%) |
|--------|-------------------------|-------------------------|---------------------------------------|------------|------------|------------|------------|--------------------------|-------------------------|--------------------------------------|---------------------------------------|------------|------------------------|------------|------------|
| MC1 | 49.89 | 0.74 | 17.84 | 8.85 | 0.14 | 6.48 | 9.96 | 3.44 | 0.35 | 0.03 | 0.0269 | 0.0072 | 0.010 | 1.42 | 99.19 |
| MC31 | 46.32 | 2.10 | 14.02 | 13.53 | 0.21 | 7.71 | 9.31 | 2.27 | 1.39 | 0.19 | 0.0237 | 0.0115 | 0.019 | 2.17 | 99.28 |

granites, and a less well-developed foliation. In some outcrops, the Kennack granites cross-cut this mafic unit, whereas in other outcrops there is streaking, interfolding and interfingering (Figures 9c and 9d). Unit 2 often contains large plagioclase xenocrysts, and patches of gabbroic texture. We interpret these textures to show that the felsic granite intruded Unit 2, likely while Unit 2 was fairly weak. This may have allowed some limited magma mingling, although many of intrusive contacts experienced subsequent ductile deformation which makes interpretation of the original intrusive nature difficult. Sandeman et al. (2000) interpreted the textures as magma comingling and mixing between felsic and mafic melts. We conclude that the mafic lithologies of Unit 1 substantially pre-date the intrusion of the granite while the mafic lithologies of Unit 2 likely pre-date the granites but were still demonstrating limited plastic behavior at the time of felsic intrusion. Dolerite dykes can also be observed intruding the Lizard peridotite and are cross-cut by the Kennack granite (Figure 9f). The sharp planar contact between the granite and the dolerite dyke shows that the felsic granite substantially postdates the dyke.

Collectively, these observations imply that the Kennack K-feldspar rich granites intruded the Lizard peridotite and metamorphic sole during the later phase of ophiolite obduction, and after the formation of the Unit 2 mafic rocks and dolerite dykes, while incorporating enclaves of the earlier Landewednack amphibolites (Figures 9a and 9b). This may be indicative of continental subduction beneath the obducted ophiolite thrust sheet, and suggests that the Kennack granites may be equivalent to many of the felsic dykes intruding the base of the mantle sequence in the Oman ophiolite (Cox et al., 1999; Rioux et al., 2021; Rollinson, 2014). The formation mechanism of the Unit 2 mafic lithology and dolerite dykes is unclear, but they must post-date spreading ridge magmatism, as both lithologies clearly intrude the Lizard peridotite, and marginally pre-date the Kennack granites. For clarity, we suggest that the felsic components of the Kennack Gneiss should be termed the Kennack granites, and the two mafic units (Unit 1, Unit 2 above) should be dealt with separately.

7. Pressure–Temperature Conditions of Metamorphism of the Metamorphic Sole

The subduction dynamics governing the formation and obduction of an ophiolite can be examined using the pressure-temperature-time (P – T – t) evolution of the metamorphic sole (e.g., Cowan et al., 2014; Guilmette et al., 2018; Soret et al., 2017). The Landewednack Amphibolites have previously been identified as the sole of the Lizard ophiolite (e.g., Cook et al., 2002; Sandeman et al., 1995). Sandeman et al. (1995) used the compositions of plagioclase-amphibole pairs with the Holland and Blundy (1994) thermometer to conclude that the Landewednack Amphibolites experienced metamorphism at conditions of c. 600°C and c. 3–4 kbar. Cook (1999) reported similar conditions of 550–700°C and 2–6 kbar by using thermobarometry applied to plagioclase-amphibole pairs (Cook et al., 2002). Nonetheless, both calibrations provide relatively poor constraints on the pressure of equilibration and carry large uncertainties that propagate through the calculation to give notable error on calculated depths of equilibration.

We used petrological modeling to constrain the conditions of metamorphism experienced by the Landewednack sole amphibolites, as they lack typical pressure-sensitive assemblages used in conventional thermobarometry. Phase diagram construction was performed using Theriak-Domino (2019) (de Capitani & Petrakakis, 2010) and database ds-62 (Holland & Powell, 2011) in the Na₂O–CaO–K₂O–FeO–MgO–Al₂O₃–SiO₂–H₂O–TiO₂–O₂ (NCKFMASHTO) system using activity–composition (a – X) relations for subsolidus and suprasolidus relations in metabasites described by Green et al. (2016). Pure phases comprised albite, quartz, rutile, sphene (titanite), and aqueous fluid (H₂O). Modeling was performed assuming fluid saturation and a bulk-rock $X_{\text{Fe}^{3+}} [\text{Fe}_2\text{O}_3/(\text{FeO} + \text{Fe}_2\text{O}_3)]$ of 0.12, which is typical of unaltered mid-oceanic ridge basalt (cf. Hernández-Urbe & Palin, 2019). The bulk compositions of samples MC1 and MC31 are given in Table 1.

While MnO imparts a strong control on the stability of garnet in metabasic rocks, the current omission of MnO from a – X relations for clinopyroxene and clin amphibole (Forshaw et al., 2019) precluded its consideration here.

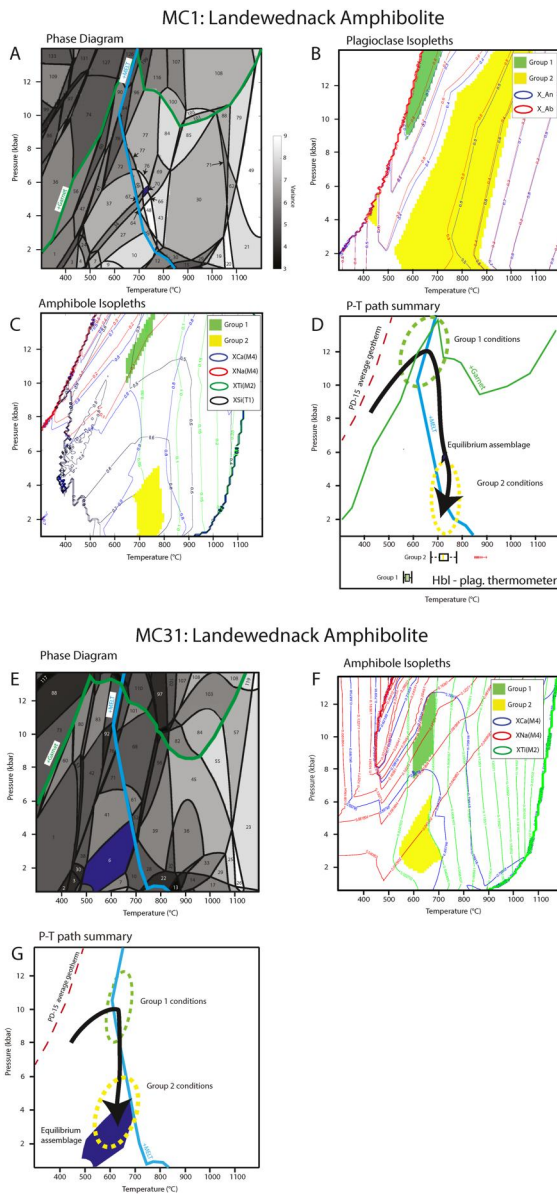


Figure 11. Equilibrium phase diagrams of the metamorphic sole (a) Phase diagram, Sample MC1; (b) Plagioclase compositional isopleths, Sample MC1. (c) Amphibole compositional isopleths, Sample MC1. (d) Summary P - T path and hornblende-plagioclase thermometer results, Sample MC1. (e) Phase diagram, Sample MC31; (f) Amphibole compositional isopleths, Sample MC31. (g) Summary P - T path, Sample MC31.

Nonetheless, measured MnO in the studied samples was lower than typical MORB (Gale et al., 2013) and its omission from the model system is not expected to affect our conclusions. The approximate uncertainty on the absolute position of phase boundaries on a typical pseudosection is $\pm 50^\circ\text{C}$ and ± 1 kbar at 1 S.D.; however, as this error largely stems from uncertainties in thermodynamic end-member data in internally consistent data sets and the validity of a - X relations, the relative uncertainty between models is significantly reduced when all use the same setup parameters (Palin et al., 2016). As such, the relative precision of our modeling reaches $\pm 20^\circ\text{C}$ and ± 0.2 kbar at 1 S.D., which allows discrimination of the relative differences in depth of burial of different units to ± 1 – 2 km at 95% confidence (Palin et al., 2016).

7.1. Landewednack Amphibolites: Sample MC1

7.1.1. Equilibrium Assemblage

A P - T pseudosection for Landewednack Amphibolite sample MC1, constructed between 300 and 1200°C and 1–14 kbar, is shown in Figure 11a. The stable phase assemblage for each field within the pseudosection is documented in Supporting Information S1. This sample was collected directly below the Lizard Thrust at Mullion Cove. We interpret that trondhjemitic melt was present during metamorphism due to domains that are enriched in coarse-grained plagioclase and quartz, which is characteristic of low-degree partial melt zones in metabasic rocks (Sawyer, 2008) (Figure 12c). Domains interpreted to represent higher degrees of partial melting are characterized by coarse amphibole crystals surrounded by plagioclase and quartz with cusped contacts and embayments (e.g., Figure 12d), which are also well-known microstructures associated with anatexis. Figures 12c and 12d highlight domains within sample MC1 of low-degree melt and high-degree melt respectively. Notably, high-degree melt domains often have a lower proportion of ilmenite, suggesting that it was consumed during melting reaction (e.g., Beard & Lofgren, 1991). Macroscopic domains of plagioclase and quartz, interpreted to represent melt pockets, were also seen in outcrop (e.g., Figures 12a and 12b). Some of these contain coarse hornblende and biotite, indicating crystallization at high temperatures as opposed to low-temperature fluid infiltration and subsolidus mineral precipitation. While the degree of melting during metamorphism is unconstrained, observations made at outcrops of the Landewednack Amphibolite throughout the peninsula suggest no more than 5–10 vol. % of melt, which correlates with thin section observation. The interpreted peak assemblage in sample MC1 of trondhjemitic melt, hornblende, plagioclase, ilmenite, titanite, and quartz (Figure 8b) is calculated to be stable at P - T conditions of 5.2–5.9 kbar and 710–735°C.

7.1.2. Phase Compositions

The chemical composition of minerals in Sample MC1 were analyzed with a CAMECA SX5-FE electron microprobe at the Department of Earth Sciences, University of Oxford, using an accelerating voltage of 15 kV and a beam current of 20 nA. Calibrations were performed using a variety of standards, including andradite (Fe, Mg, and Ca), labradorite (Na, Al, and Si), TiO_2 (Ti), Mn metal (Mn), and sanidine (K). Data for amphibole and plagioclase are plotted in Figure 10 with all other mineral compositions presented in Supporting Information S1.

All amphibole compositions lie within the magnesio-hornblende field of Leake et al. (1997) (Figure 10e), however principal component analysis (PCA) reveals two clear groups (Figure 10d). This is supported by the petrography, which clearly shows two generations of amphibole (Figure 8c) and a conventional Na(M4) atoms per formula unit plot after Schumacher (2007) (Figure 10f). In addition, plagioclase showed a wide range of

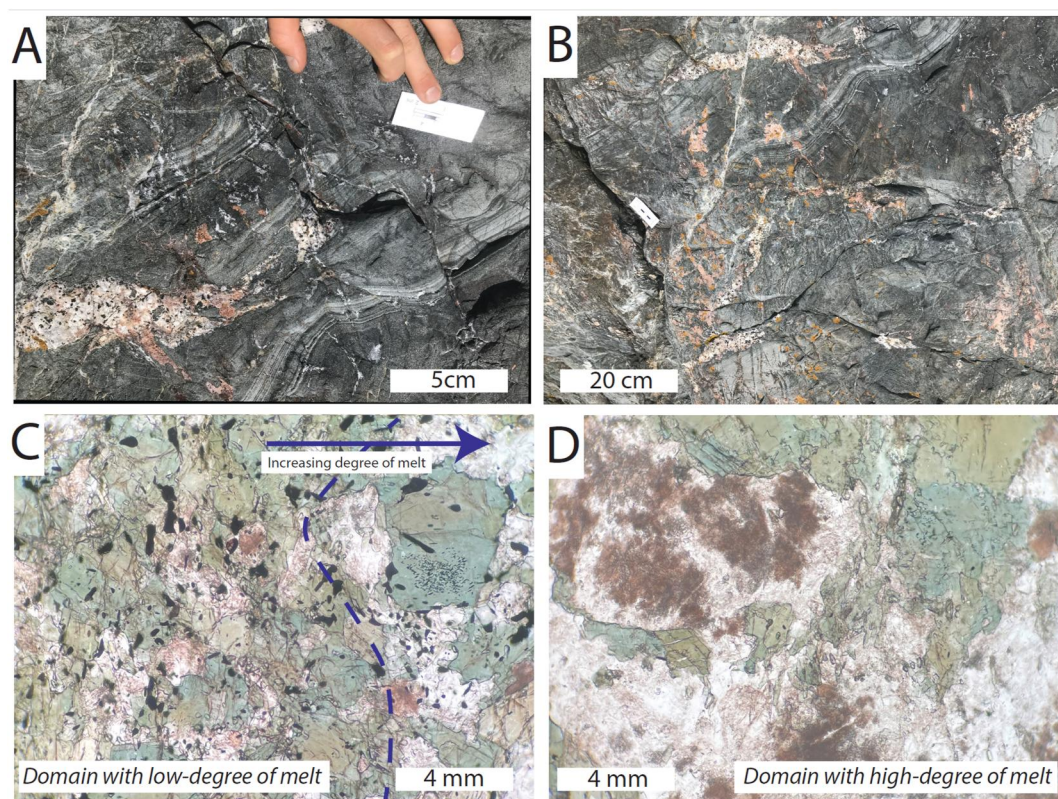


Figure 12. Evidence of partial melting in the Landewednack Amphibolites. (a) Landewednack Amphibolite (Housel Bay); (b) Landewednack Amphibolite (Porthkerris); (c) Petrograph of a Landewednack Amphibolite, Sample MC1, showing domains of contrasting melt proportions; (d) Petrograph of a Landewednack Amphibolite, Sample MC1, showing a domain with a relatively high proportion of melt.

compositions, spanning the range X_{Ab} $[Na/(Na + Ca + K)] = 0.4\text{--}0.9$. Like the amphiboles, the plagioclase can also be separated into two key groups: Group 1 lies within the labradorite—andesine fields, and Group 2 lies within the oligoclase—albite fields. We compared the forward-calculated composition of amphibole and plagioclase at different P - T conditions with the observed compositions of both chemically distinct amphibole groups, and both plagioclase groups. The site parameters Ca (M4), Na(M4), Ti(M2), and Mg(M13) for amphibole, and the anorthite content of the plagioclase were chosen due to their sensitivity to P and/or T variation. The Group 1 plagioclase plot at conditions of 10+ kbar and 550–700°C (Figure 11b), which overlaps with the conditions experienced by the Group 1 amphibole of 10+ kbar and 650–750°C (Figure 11c). Likewise, the Group 2 plagioclase overlap with the Group 2 amphibole at lower temperature and pressures. The results indicate that Groups 1 and 2 are predicted to stabilize in two distinct regions of P - T space: a high-pressure/low-temperature and a low-pressure/high-temperature region, respectively. These results suggest decompression from peak conditions of 10+ kbar and 550–700°C to 2–5 kbar and c. 700–800°C (Figure 11d). The latter is in agreement with the present-day equilibrium phase assemblage (purple field within Figure 11d) and demonstrates that the phases stable within the region defined by the Group 1 minerals have been entirely overprinted by the later Group 2 assemblage. For example, the clinopyroxene predicted to be stable with the Group 1 minerals (e.g., Field 90 on Figure 11a) has retrogressed to amphibole in the presence of water. No garnet relicts remain, suggesting that the rock did not enter the garnet-stable field at any point within its P - T history.

7.1.3. Plagioclase-Amphibole Thermometer

The edenite-tremolite CaAl—NaSi exchange thermometer of Holland and Blundy (1994) was applied to the plagioclase—amphibole mineral pairs in Sample MC1, to confirm the results from the equilibrium modeling. The Group 1 and Group 2 minerals were analyzed separately, as they have been shown to preserve different points in P - T space. The results were calculated using the Excel-based tools developed by Hora et al. (2013), and we

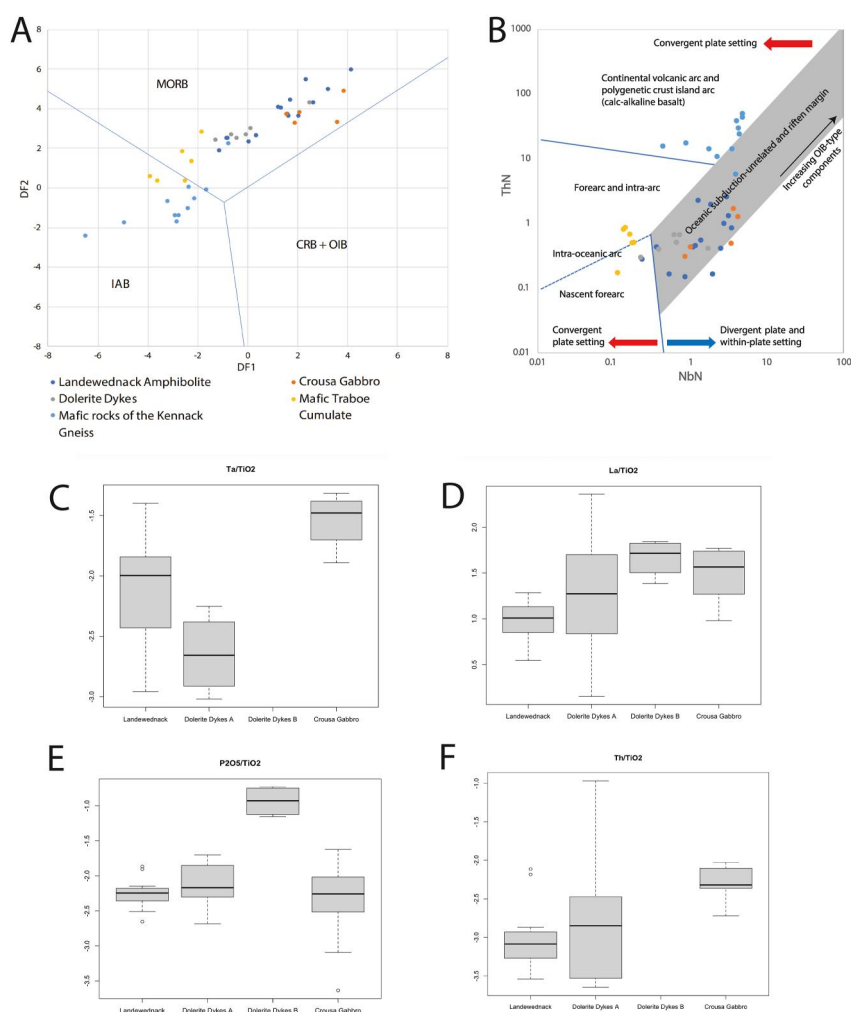


Figure 13. (a) Geochemical function diagram for tectonic discrimination of the mafic units of the Lizard Peninsula (after Agrawal et al. (2008)); (b) Th_N-Nb_N tectonic discrimination diagram of mafic units of the Lizard Peninsula (after Saccani (2015)); (c–f) Boxplots of log-transformed immobile trace element ratios data from the Landewednack Amphibolites, two groups of dolerite dykes and the Crousa Gabbro.

created boxplots of the resulting temperatures for the different mineral pairs (Figure 12d). The Group 1 mineral pairs have a median temperature of 574°C ($2\sigma = 25^\circ\text{C}$) and the Group 2 mineral pairs have a median temperature of 721°C ($2\sigma = 44^\circ\text{C}$). These temperature ranges overlap well with those predicted from the equilibrium modeling.

7.2. Mafic Sample Within the Old Lizard Head Series: Sample MC31

7.2.1. Equilibrium Assemblage

A complementary sample of sheared amphibolite (MC31) was collected from a thin sheet of meta-mafic material within the Old Lizard Head Series greenschist metamorphic sole near Predannack. The sample is a fine-grained (mean grain size of <0.25 mm) ultramylonite with a foliation defined by amphibole, quartz and plagioclase. The peak assemblage is plagioclase, amphibole, quartz, ilmenite and biotite (purple field in Figures 11e and 11g), although biotite has largely been retrogressed to chlorite. A small portion of clinopyroxene is predicted in the equilibrium models but is not observed in thin section. This is a well-known issue with parameterization of the augite activity-composition model of Green et al. (2016), but it does not affect the stability of other major phases (e.g., Forshaw et al., 2019). The peak assemblage was calculated to have formed between 1 and 5 kbar and 500–700°C.

7.2.2. Phase Compositions

Mylonitization involves pervasive recrystallization and a reduction in average grain size, such that any equilibrium assemblage present prior to shearing should re-equilibrate at the new P - T conditions of deformation. Mineral compositions are also prone to be reset during this process. The compositions of the amphibole and plagioclase crystals for sample MC31 are shown in Figures 10b and 10g–10j. The plagioclase crystals form one population with high albite contents. These clearly represent an alteration of original plagioclase compositions and are not considered further. The amphiboles are magnesio-hornblende and unlike sample MC1, they cannot be readily split into groups based on conventional amphibole composition plots. However, the amphiboles can be clearly split into two groups based on Principal Component Analysis (Figure 10g). The compositions of the two groups are compared to the model predicted compositions in Figure 11f. As in Sample MC1, two distinct regions of P - T space are preserved in the sample. The Group 1 amphiboles preserve a medium-pressure, low-temperature chemistry (8–12 kbar, 600–700°C) which formed at similar conditions to the Group 1 amphiboles of sample MC1 (Figure 11f). The Group 2 amphiboles preserve a low-pressure, high-temperature composition (2–6 kbar, 550–700°C), which again formed at similar conditions to the Group 2 amphiboles in sample MC1. As mentioned above, mylonitization acts to reset mineral chemistry during deformation. We therefore consider two separate models to explain the existence of two groups of amphibole compositions: (a) mylonitization occurred near peak conditions (in which Group 1 high- P amphiboles were formed), and then the later, low- P retrogression (which formed the Group 2 amphiboles) was chemically extensive but largely post-kinematic, since no new pervasive fabric developed; (b) the Group 1 (higher pressure) amphiboles formed post-mylonitization, and are anomalies representing disequilibrium. We favor Option 1 for two reasons: first, the sample does not display a pervasive lattice-preferred-orientation and therefore suggests significant chemical re-equilibration post-shearing; and second, the preserved P - T path is the same path as that experienced by sample MC1 (compare Figures 11d–11g).

8. Whole-Rock Geochemistry

The geochemistry of the mafic and ultramafic units of the Lizard Ophiolite has been examined in a number of studies. Davies (1984) carried out trace element and isotope analysis on the Lizard peridotites and dolerite dykes and found that the peridotites were enriched in trace-elements whereas the dykes were MORB-like. He concluded that the Lizard complex was comparable to the development of the Red Sea, with early trace-element enriched magmatism followed by MORB-magmatism. This conclusion was supported by Cook et al. (2000), following their study on the Fo and Cr values of the Lizard spinel lherzolites, and by Roberts et al. (1993). A Gulf of California atypical back-arc-basin model was proposed by Floyd (1995) to explain the geochemical variation exhibited by the Lizard ophiolite dykes and the metabasalts contained as clasts within the Roseland Breccia Formation. Cook (1999) found the Landewednack Amphibolites to have a T-MORB signature, but divided the amphibolites into two groups, Landewednack and Porthoustock, based on their REE element geochemistry (Cook et al., 2000). Given the identical structural position of these two groups, we suggest that the geochemical variations reflect lithological variation within the amphibolite protolith, and we therefore do not treat them separately. We use “Landewednack Amphibolite” to describe occurrences of both Landewednack Amphibolite and Porthoustock Amphibolite. The mafic units of the Kennack Gneiss were studied by Sandeman et al. (2000), who concluded that the mafic rocks had an E-MORB signature, potentially derived from spreading in an off-axis environment marginal to a mantle plume. However, E-MORB is not necessarily a sign of mantle plume involvement (Gale et al., 2013).

Despite this existing work, questions still exist around the similarity between the Landewednack amphibolites and the mafic rocks of the Lizard ophiolite. Could the mafic rocks of the Lizard ophiolite represent the protoliths of the amphibolites? To answer this, geochemical data from Kirby (1979), Sandeman (1988), Roberts et al. (1993), Sandeman et al. (1997), and Cook (1999) was compiled in order to re-examine the geochemical signatures of the rocks from the Lizard ophiolite using the maximum number of analyses available. Tectonic discrimination diagrams based on immobile elements can distinguish the tectonic settings of ophiolites. For example, the boninitic (high Mg andesite) island-arc affinity of the Oman ophiolite pillow basalts clearly demonstrates that they formed above an active subduction zone (Pearce et al., 1981). Immobile elements must be used because extensive hydrothermal alteration and weathering after ophiolite formation obscures the mobile element signature (Pearce, 2014).

Table 2
Mann-Whitney Test of Ophiolitic Mafic Rocks and the Landewednack Amphibolites

| LOG ratio | LA—CG | | LA—DOLA | | LA—DOLB | |
|---|----------|-------------|---------|-------------|----------|-------------|
| | P value | W-statistic | P value | W-statistic | P value | W-statistic |
| MnO/TiO ₂ | 0.1087 | 78 | 0.7804 | 224 | 0.007018 | 49 |
| P ₂ O ₅ /TiO ₂ | 0.9046 | 93 | 0.05929 | 109 | 0.000516 | 0 |
| Zr/TiO ₂ | 0.7587 | 104 | 0.00187 | 82 | 0.002064 | 48 |
| Y/TiO ₂ | 0.5169 | 93 | 0.01584 | 100 | 0.008256 | 1 |
| Nb/TiO ₂ | 0.1086 | 51 | 0.1308 | 127 | 0.006192 | 4 |
| Yb/TiO ₂ | 0.8411 | 45 | 0.2667 | 39 | nan | nan |
| Hf/TiO ₂ | 0.1869 | 81 | 0.07495 | 110 | nan | nan |
| Ta/TiO ₂ | 0.02735 | 8 | 0.0485 | 50 | nan | nan |
| Th/TiO ₂ | 0.006769 | 6 | 0.8596 | 49 | nan | nan |
| La/TiO ₂ | 0.002123 | 11 | 0.06636 | 116 | 0.000516 | 0 |
| Sm/TiO ₂ | 0.9096 | 43 | 0.01835 | 15 | nan | nan |

The Landewednack Amphibolites of the metamorphic sole have a clear MORB signature, lying in the MORB field of the function diagram (Figure 13a) and the Th_N–Nb_N discrimination diagram (Figure 13b). This is consistent with the hypothesis that the protoliths of the metamorphic sole formed during a period of spreading in the Rheic-Rhenohercynian ocean prior to the onset of subduction. The Crousa gabbro and associated dolerite dykes of the ophiolite also plot almost exclusively within the MORB field of the function diagram (Figure 13a) and the oceanic subduction-unrelated and rifted margin field of the Th:Nb diagram (Figure 13b). These conclusions support the work referenced in Section 4.2. However, the mafic Traboe Cumulates have an intra-oceanic arc signature (Figure 13b), and the mafic units of the Kennack Gneiss have a clear island-arc signature (Figures 13a and 13b). This suggests an evolution from MORB geochemistry to arc-like geochemistry through time.

Finally, we compared the geochemistry of the ophiolite mafic rocks (Crousa Gabbro and dolerite dykes) with the metamorphic sole (Landewednack Amphibolites) using a combination of boxplots and the Mann-Whitney test (Mann & Whitney, 1947). This test assesses whether two groups of samples have come from the same population. The null hypothesis stipulates that the distributions of the two populations sampled are identical, and therefore the two groups have come from the same population. Consequently, to prove that the Landewednack Amphibolites are geochemically distinct from the ophiolite rocks, the null hypothesis would have to be rejected. The Mann-Whitney test is a non-parametric statistic and is therefore well suited to these data which often have a non-Gaussian distribution. The assumptions of the test are that the two groups are independent, the dependent variables are continuous and that the distributions of the dependent variables are similar between the three groups (which is evident from the boxplots in Figure 13). The compiled geochemical data permitted the use of the immobile element compositions (TiO₂, MnO, P₂O₅, Zr, Y, Nb, Yb, Hf, Ta, Th, La, Sm) for 17 samples of Landewednack Amphibolite (LA), 29 samples of dolerite dykes and 14 samples of Crousa Gabbro (CG). The dolerite dykes were split into Group A (DOLA) and Group B (DOLB), due to the clear geochemical differences between the groups (e.g., Figure 13e). Some samples did not have data available for every element (e.g., Dolerite Dykes B in Figures 13c and 13f), in which case the sample was ignored for that element analysis. To enable a robust analysis, we performed an additive log-ratio transformation on the data set, following Rollinson and Pease (2021): For every sample, we normalized the element concentrations to the TiO₂ concentration of that sample. The natural logarithm of each element ratio was taken, and outliers (lower bound = Q1 – 1.5*IQR; upper bound = Q3 + 1.5*IQR) were removed. The Mann-Whitney test was applied to this transformed data set, and the results are summarized in Table 2.

A p-value below 0.05 indicates that the null hypothesis can be rejected with a certainty of >95%, and therefore assert that the rock types are geochemically distinct. The results in Table 2 show that the Ta/TiO₂, Th/TiO₂, and La/TiO₂ ratios of the Landewednack Amphibolites are geochemically distinct from the Crousa Gabbro. This is clear when examining the salient boxplots (Figures 13c–13f). The Landewednack Amphibolites are also distinct

from Group B dolerite dykes and vary significantly from the Group A dolerite dykes (Zr/TiO₂, Y/TiO₂, Ta/TiO₂, and Sm/TiO₂). This is clearly supported by the ratio boxplots. Consequently, we conclude that the Landewednack Amphibolites are geochemically distinct from the ophiolite rocks and therefore could not have formed from metamorphism of the ophiolite. This supports the hypothesis that the Landewednack Amphibolites are part of a subduction-zone metamorphic sole.

9. Geochronology

Our field observations and *P-T* analyses are supported by new chemical abrasion isotope dilution thermal ionization mass spectrometry (CA-ID-TIMS) U-Pb dates, obtained from two units, following method described by Tapster et al. (2016). One sample was also dated by laser ablation inductively coupled plasma mass spectrometry (LA-ICP-MS), following the method described in Roberts et al. (2011), to screen for any inheritance within the separated zircon population. The data and methods are provided in Supporting Informations S1 and S2.

9.1. Previous Geochronology

The age of the Lizard ophiolite has been a subject of considerable debate. Igneous and high-temperature metamorphism zircon dates are primarily reported by Sandeman et al. (1997), Clark et al. (1998), and Nutman et al. (2001, 2023). However, the previously unclear geological and structural characterization of the various Lizard units, and the significance of the data itself have prevented a clear interpretation of zircon U-Pb ages. For example, a ²⁰⁷Pb/²⁰⁶Pb date of 397 ± 2 Ma was reported for a “plagiogranite” sample at Porthkerris (Clark et al., 1998). However, the lithological association of this date is unclear, and it has been debated whether the sample represents, (a) a true plagiogranite (the last phase of fractional crystallization from the ophiolite), and should therefore be attributed to ophiolite formation, (b) partial melting of Traboe Cumulate rocks at granulite facies conditions, (c) granites of the Kennack Gneiss (see discussion of Clark et al. (2003)) or (d) partial melting within the Landewednack Amphibolites of the metamorphic sole. The field location reported does not provide sufficient locality detail to be able to evaluate the nature of the unit dated. Second, the interpretation of the data itself can also be challenged. The date of 397 ± 2 Ma is based on three ²⁰⁷Pb/²⁰⁶Pb air-abraded ID-TIMS analyses of zircon. Our own analysis shows that the three dates lie within uncertainty of concordia, yet only two dates show repeatable ²⁰⁶Pb/²³⁸U dates with a weighted mean of 398.28 ± 0.50 Ma (2s). The remaining analysis yields an apparently younger date of 395.66 ± 0.76 Ma (2s) (Supporting Information S1). It is unclear whether this younger date relates to a younger zircon growth event at ca. 395 Ma, or whether it merely reflects open system behavior with respect to Pb. Any younger Pb-loss event would generate trajectories that were sub-parallel to concordia and would therefore not be resolvable as a discordant analysis at the precision of the U-Pb data. Given the field description (“collected from a swarm of thin veins from an outcrop...the host-rocks are laminated mylonites, representing both Landewednack- and Traboe-type hornblende schists”) and the approximate sample location provided by Clark et al. (2003), we believe that the “plagiogranite” sample was actually a sample of Landewednack amphibolite with melt sweats (i.e., metamorphic sole), and we consequently interpret the 398–395 Ma age to reflect partial melting and incipient cooling of the Landewednack Amphibolite metamorphic sole.

Many of the previously reported U-Pb data for the Lizard lithologies were obtained via ion microprobe (SHRIMP) analysis (Nutman et al., 2001, 2023). Whilst ages of ophiolite-related units cluster in the Upper Devonian around ~390 Ma, the associated 2s uncertainties of the data (typically ± 20–30 Myrs) are prohibitive to interpretation at the timescales of the geological processes and many samples yield complex common-Pb, and potentially Pb-loss related behavior that permit multiple interpretations. The previously reported ²⁰⁶Pb/²³⁸U date for the Landewednack Amphibolite (Hornblende Schist; 96/543, Nutman et al., 2001) was 379 ± 25 Ma (2s). Recalculation of a Tera-Wasserburg lower intercept date, with a free regression yields a U-Pb date of 396 ± 39 Ma (Supporting Information S1). The magnitude of the associated uncertainty indicates the data are inadequate for interrogating the chronology of Lizard Ophiolite formation beyond a general indication of its Devonian age. It therefore calls for better constraints to define the formation model.

Comparable issues with the limitation of data interpretation for resolving the geological model due to stated uncertainty level are documented across the reported SHRIMP U-Pb dates reported by Nutman et al. (2001). Two samples described as Traboe hornblende schists from the west coast of the Lizard were dated with U-Pb zircon by Nutman et al. (2001). One sample from Predannack Head containing hbl + cpx + pl + il yielded a date of 393 ± 6 Ma; the other sample described as a granulite, contains opx + cpx + pl + il, and was reported with a date

of 386 ± 7 Ma (Nutman et al., 2001). Recalculation of these dates (Supporting Information S1) yields a Tera-Wasserburg lower intercept date of 388.0 ± 7.6 Ma, or a $^{206}\text{Pb}/^{238}\text{U}$ weighted mean of 394.7 ± 7.6 Ma from the most concordant analyses; either 384.0 ± 6.8 Ma (Tera-Wasserburg lower intercept date) or 390.0 ± 7.1 ($^{206}\text{Pb}/^{238}\text{U}$ weighted mean of the most concordant data points); and either 382.8 ± 9.0 (Tera-Wasserburg lower intercept date) or 384.1 ± 8.4 Ma ($^{206}\text{Pb}/^{238}\text{U}$ weighted mean of the most concordant data points). We suggest these support an argument for Traboe Cumulate formation that seems to cluster around 390–380 Ma. As discussed in Section 4.4, we follow Styles and Kirby (1980) in interpreting the Traboe Cumulate formation as part of the ophiolite sequence. Consequently, the 390–380 Ma cluster of Traboe ages suggests that ophiolite spreading occurred over a prolonged time period during the Mid-Devonian. Nutman et al. (2001) also report an age of 387 ± 7 Ma for metagabbro belonging to either the Landewednack or Traboe Hornblende Schists; however, given the geological uncertainty of this sample, we do not consider it further.

However, these in situ U-Pb data are useful for the interpretation of inherited zircon components within units. For example, detrital zircons from a biotite schist layer within the Landewednack amphibolite have an age of 500 Ma, and detrital zircons from the Traboe Cumulate complex have a spread of ages from 473 ± 3 to 502 ± 23 Ma (Nutman et al., 2001). These detrital zircon ages give maximum ages of their respective units, and broadly overlap with the zircon U-Pb ages of $499 \pm 8/-3$ and from the Man of War Gneiss (Sandeman et al., 1997) and c. 500 Ma granodioritic bodies in the Old Lizard Head Series (Nutman et al., 2001, 2023), respectively. Magmatism of this type at around 500 Ma typifies the peri-Gondwanan region (Sandeman et al., 1997). Likewise, a small component of potentially younger, post-Devonian dates was identified within rim domains and was attributed to Pb-loss during a later thermal event (Nutman et al., 2001). This may coincide with the local expressions of the Variscan orogeny.

Whilst the Kennack Gneiss (i.e., Kennack granites, see Section 6) is not the primary focus of this study, both ion microprobe and ID-TIMS zircon U-Pb data was previously obtained from units of the Kennack Gneiss (Nutman et al., 2001; Sandeman et al., 2000). The ID-TIMS yielded complex data with all 4 analyses indicating discordance at variable uncertainty levels. The seemingly precise date for this unit was inferred from a lower intercept ($^{207}\text{Pb}/^{206}\text{Pb}$ equivalent) date of 376.4 ± 1.4 Ma, interpreted on the basis that dates fall along a binary mixing trend with a ~ 2 Ga inherited component. However, only three of the four data points lie within uncertainty of this trajectory, and one analysis has large associated uncertainties. Therefore, this date is effectively based upon a two-point isochron and is not a robust constraint. As indicated within previous discussions (Clark et al., 2003), this approach to age interpretation permits that the reported date is highly subject to whether open-system behavior is present, and we note this study was conducted prior to the modern chemical abrasion approaches to Pb-loss reduction that we adopted for the new data of this study. However, the alternative age interpretation, that suggests the data can be described by Pb-loss of an older ~ 390 Ma event, provided within Clark et al. (2003) is erroneous, as it results in an unfeasible negative lower intercept age, rather than a zero or positive age, and as a result yields meaningless regressions with regards to the age of the Kennack Gneiss sample. Conversely the SHRIMP U-Pb data of Nutman et al. (2001) indicate a nominally older timing of >390 Ma, yet with similar caveats regarding the single data point precision and the geological uncertainty preventing a clear interpretation of zircon U-Pb ages from these units. In the simplest terms, none of the current U-Pb data available from the Kennack Gneiss permits discrimination between either interpretation (~ 390 or ~ 376 Ma).

New magmatic zircon ages were reported for several lithologies by Nutman et al. (2023). These ages can be separated into three suites: (a) a 498 ± 11 – 488 ± 9 Ma suite recorded in the Man of War Gneiss and granodiorite sheets within the Old Lizard Head Series; (b) a 482 ± 12 – 478 ± 12 Ma suite preserved in the Landewednack Amphibolites and the Traboe Hornblende Schist; and (c) a 393 ± 11 – 391 ± 10 Ma suite preserved in the Crousa Gabbro and “felsic sheets within peridotite” respectively. The first suite represents continental magmatism occurring prior to, or during the early stages of continental rifting. We suggest that the granodiorite sheets within the Old Lizard Head Series may represent submarine felsic lava flows, which are common on continental and transitional crust (Reynolds et al., 2017; White et al., 2015). The second suite represents the formation of the new oceanic crust, during which the protolith for the Landewednack Amphibolites was formed. As discussed in Section 4.4, some samples of the Landewednack Amphibolites did not experience partial melting, so the zircon ages will represent original magmatic ages. The lithological description of the “Traboe” sample (sample 97–277) given by Nutman et al. (“*fine-grained green-brown hornblende + plagioclase amphibolite with a sub-vertical foliation*”) describes a strongly deformed metamorphic rock, whereas we interpret the Traboe Cumulates as igneous rocks belonging to the Lizard ophiolite itself, such as those seen at Porthkerris. As such, we suggest that

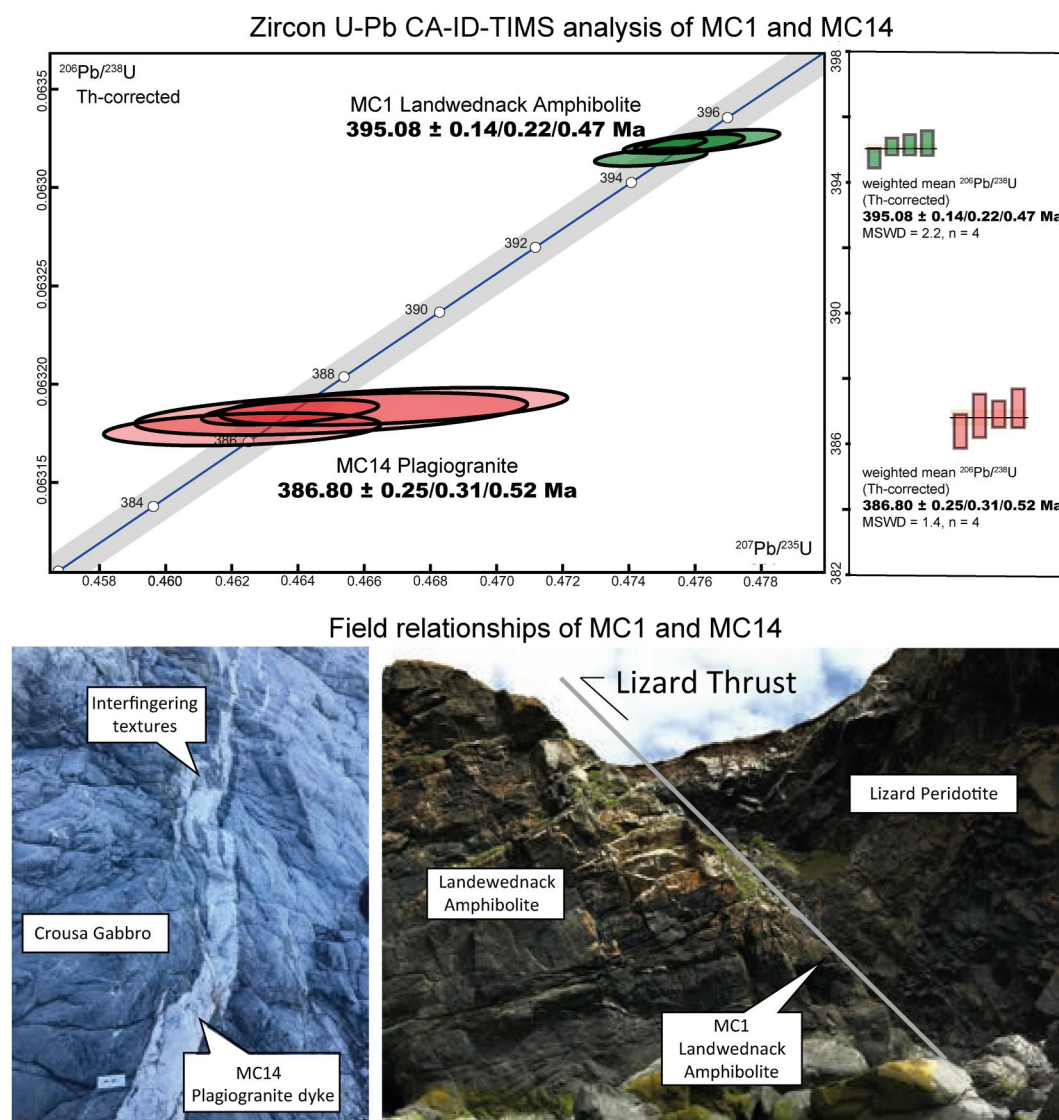


Figure 14. Concordia diagram, with field relationships, of Sample MC1 (Landwednack Amphibolite, Mullion Cove) and Sample MC14 (Plagiogranite dyke, Porthoustock) from CA-ID-TIMS analysis.

sample 97–277 belongs to the metamorphic sole and therefore the similarity in ages between the Landwednack (482 ± 12 Ma) and sample 97–277 (478 ± 12 Ma) makes sense. The final suite of ages represents the formation of the Lizard ophiolite, although the low precision on the ages prevents a more detailed tectonic interpretation. The felsic sheets within the peridotite reported by Nutman et al. (2023) are likely to be genetically linked to the Kennack Gneiss. In which case, the ~ 390 Ma age for the Kennack Gneiss (discussed above) may be more appropriate. As well as a zircon date of 393 ± 11 Ma that Nutman et al. (2023) argue represents metamorphic recrystallization, these authors also present a U-Pb baddeleyite date of 416 ± 17 Ma for the Crousa Downs Gabbro. Several issues are highlighted with both the calibration of these baddeleyite data, and with the grains themselves (Nutman et al., 2023). In addition, recalculation of the data using only the most pristine grain reveals weighted mean $^{206}\text{Pb}/^{238}\text{U}$ dates with large uncertainties (>20 Myrs; Supporting Information S1), and thus we choose to omit the baddeleyite data from our stated age range above.

9.2. Zircon CA-ID-TIMS U-Pb Age of the Lizard Ophiolite

A new U-Pb zircon (ID-TIMS) age obtained from a plagiogranite dyke (Sample MC14) is interpreted as dating the crystallisation age of the crustal sequence of the Lizard ophiolite. This plagiogranite intrudes the Crousa

Gabbro just below the sheeted dyke complex at Porthoustock and similar plagiogranites southwards to Godrevy Cove are mingled with dolerite dykes. The plagiogranites are interpreted as representing high degrees of fractional crystallisation of basaltic magma at the ridge axis. The interfingering of the dykes indicates that the plagiogranite intruded the Crousa Gabbro while it was still deforming plastically (Figure 14). Consequently, the plagiogranite is essentially coeval with the Crousa Gabbro and sheeted dykes, and an age determination from Porthoustock would constrain the latest crustal accretion at the ridge axis preserved within the Lizard ophiolite (e.g., Roberts et al., 1993).

Zircon grains from this sample were typically euhedral with aspect ratios of 3:1–4:1 and yielded a CA-ID-TIMS $^{206}\text{Pb}/^{238}\text{U}$ (Th corrected) date of $386.80 \pm 0.25/0.31/0.52$ Ma, $n = 4$, MSWD = 1.4, where 2s uncertainties are stated in the form analytical only/analytical plus tracer calibration/all uncertainty including the ^{238}U decay constant for comparison with other decay systems. Therefore, this study can conclude that the latest ocean spreading preserved within the Lizard occurred at 386.80 ± 0.52 Ma (early Givetian, Middle Devonian).

9.3. Zircon CA-ID-TIMS U–Pb Age of the Metamorphic Sole

The Landewednack Amphibolites make up the amphibolite-facies section of the metamorphic sole of the ophiolite. If amphibolites are heated above the solidus during metamorphism, amphibole-dehydration melting drives the production of pockets of melt throughout the rock. Zircon crystals within these crystallized melt pockets date the incipient cooling of these melt pockets, and consequently the time at which the amphibolites experienced cooling after peak metamorphism.

A sample of Landewednack Amphibolite (Sample MC1) was collected from directly beneath the Lizard Thrust at Mullion Cove to constrain the time at which the metamorphic sole of the Lizard ophiolite experienced incipient cooling following metamorphism and partial melting (Figure 14). A consistent euhedral habit and simple oscillatory zonation is clearly observed across the zircon grains obtained from this sample (see Supporting Information S1), compatible with an origin through partial melting of the amphibolite.

The LA-ICP-MS data from this sample, comprising 14 spots across both grain interiors and regions toward the rims, are unresolvable at the level of precision forming a weighted mean age of 392.78 ± 6.15 Ma (Figure 14). This date is comparable to that reported by the work of Nutman et al. (2001) for a sample of Landewednack Hornblende Schist (sample 95/543) analyzed by microbeam techniques (see Section 7.1). Analysis of four zircon grains extracted from the imaged epoxy mount yielded a CA-ID-TIMS U–Pb zircon age of $395.08 \pm 0.14/0.22/0.47$ Ma, with a statistically acceptable MSWD at the 95% confidence interval of 2.2. As such, we can conclude that the Landewednack Amphibolite, interpreted as the metamorphic sole of the Lizard ophiolite, experienced partial melting, metamorphism and then incipient cooling at 395.08 ± 0.47 Ma (late Emsian, Lower Devonian). This incipient cooling, during which the zircon crystallized could have occurred contemporaneously with, or potentially up to 10 Myrs after, peak metamorphism (e.g., Agard et al., 2020; Guilmette et al., 2018; Soret et al., 2022).

10. Discussion

10.1. Evidence of a Supra-Subduction Zone Origin for the Lizard Ophiolite

The Landewednack Amphibolites experienced peak metamorphic conditions of 10 ± 2 kbar and $600 \pm 75^\circ\text{C}$, followed by decompression and heating to conditions of $2\text{--}5$ kbar and $721 \pm 44^\circ\text{C}$. This is remarkably similar to the highest-grade section of other metamorphic soles (Agard et al., 2016; van Hinsbergen et al., 2015), and corresponds to 30–40 km of burial. Unsurprisingly, therefore, these conditions also match well with those expected for a subduction zone, as demonstrated by the global mean of Phanerozoic subduction zones reported by Penniston-Dorland et al. (2015) (PD15). The decompression from peak conditions and accompanying heating corresponds to exhumation of the sole and accretion to the base of the overlying ophiolite. The lower temperatures achieved by the Group 2 minerals of sample MC31 from the Old Lizard Head Series ($550\text{--}700^\circ\text{C}$, Figure 11g), in comparison to sample MC1 of the Landewednack amphibolites ($721 \pm 44^\circ\text{C}$ (2σ)), demonstrates that the Old Lizard Head Series reached a shallower level in the subduction zone compared to the Landwednack amphibolites prior to final emplacement.

The Landewednack Amphibolites have a MORB geochemistry, which suggests that their protolith formed at a spreading ridge prior to the onset of subduction. The Crousa Gabbro and associated dolerite dykes of the

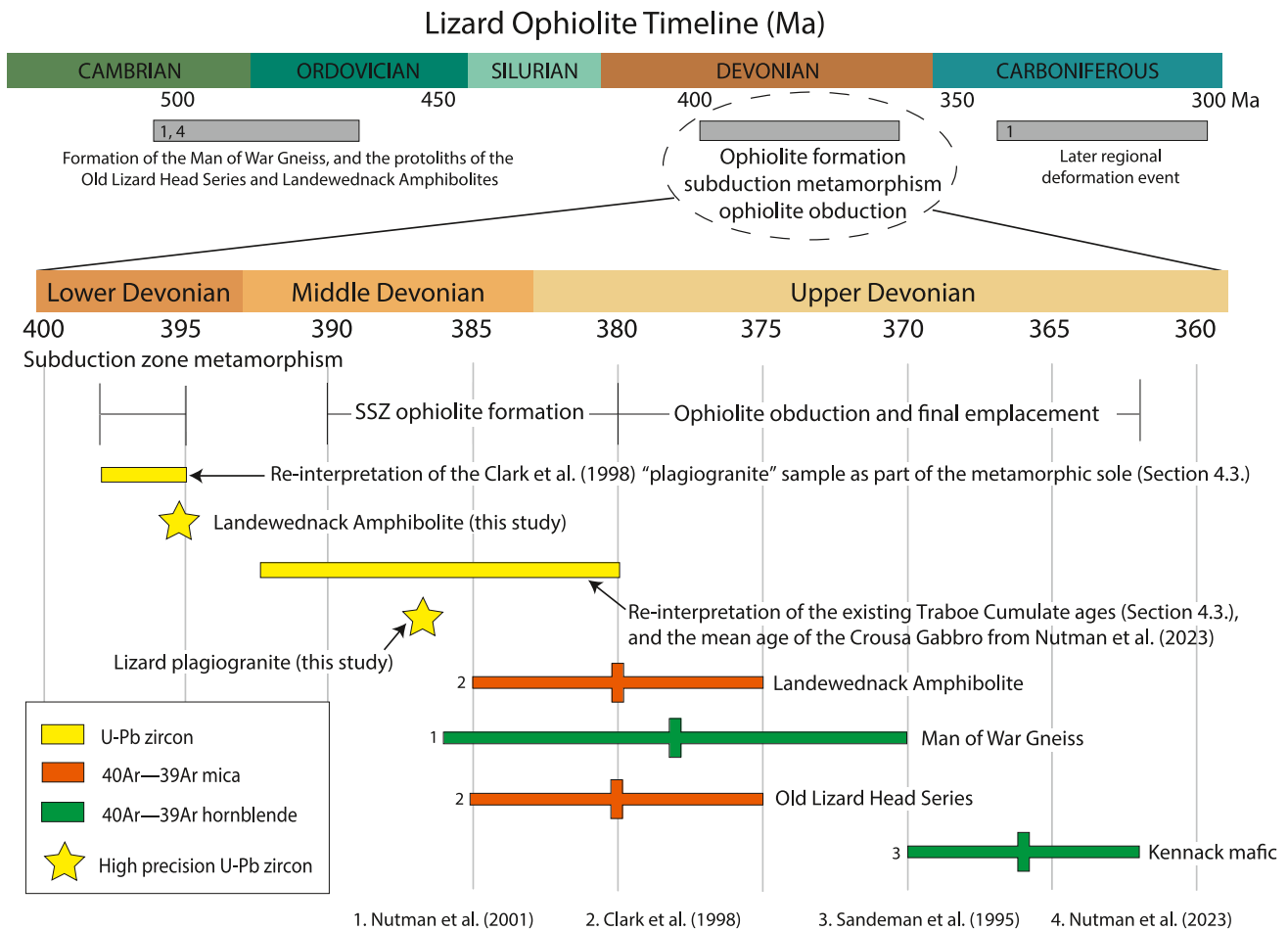


Figure 15. Geochronological timeline for the Lizard ophiolite.

ophiolite also have a MORB-like geochemistry, whereas the Traboe Cumulate sequence displays a strong arc geochemistry. We interpret this transition from MORB- to arc-like geochemistry to reflect the growing influence of the new subduction zone on the geochemistry of the ophiolite. A comparison between the ophiolite mafic rocks and the Landewednack Amphibolite using boxplots and a Mann-Whitney test of log-transformed immobile element ratios demonstrates that the mafic rocks from the ophiolite could not have been the protolith of Landewednack Amphibolite. This is only consistent with a supra-subduction zone ophiolite.

10.2. Temporal Evolution of the Lizard Ophiolite

A summary of the Lizard geochronology, using zircon U-Pb data from this study and previous work is presented in Figure 15. The Man of War Gneiss contains igneous zircons with ages of c. 500 Ma (Nutman et al., 2001; Sandeman et al., 1997) and 498 ± 11 (Nutman et al., 2023), and is interpreted as representing the formation of a continental arc during the Cambrian (e.g., Sandeman et al., 1997). This is supported by the 488 ± 9 Ma igneous zircon ages of felsic units within the Old Lizard Head Series (Nutman et al., 2023). Although previously interpreted as igneous intrusions into a basement block of Old Lizard Head Series, we interpret these felsic units as either intrusions or lava flows within the sediment protoliths of the Old Lizard Head Series. The abundance of c. 500 Ma magmatic and detrital zircons is evidence of widespread magmatism during the Cambrian and typifies the peri-Gondwanan region (Sandeman et al., 1997).

The oceanic crust protolith of the Landewednack Amphibolites formed between 482 ± 12 and 478 ± 12 Ma (Nutman et al., 2023). Partial melt sweats within the unit, interpreted to represent partial melting during subduction-zone metamorphism (Section 7), experienced incipient cooling between 398 and 395 Ma (our re-

Tectonic model for the Lizard Ophiolite

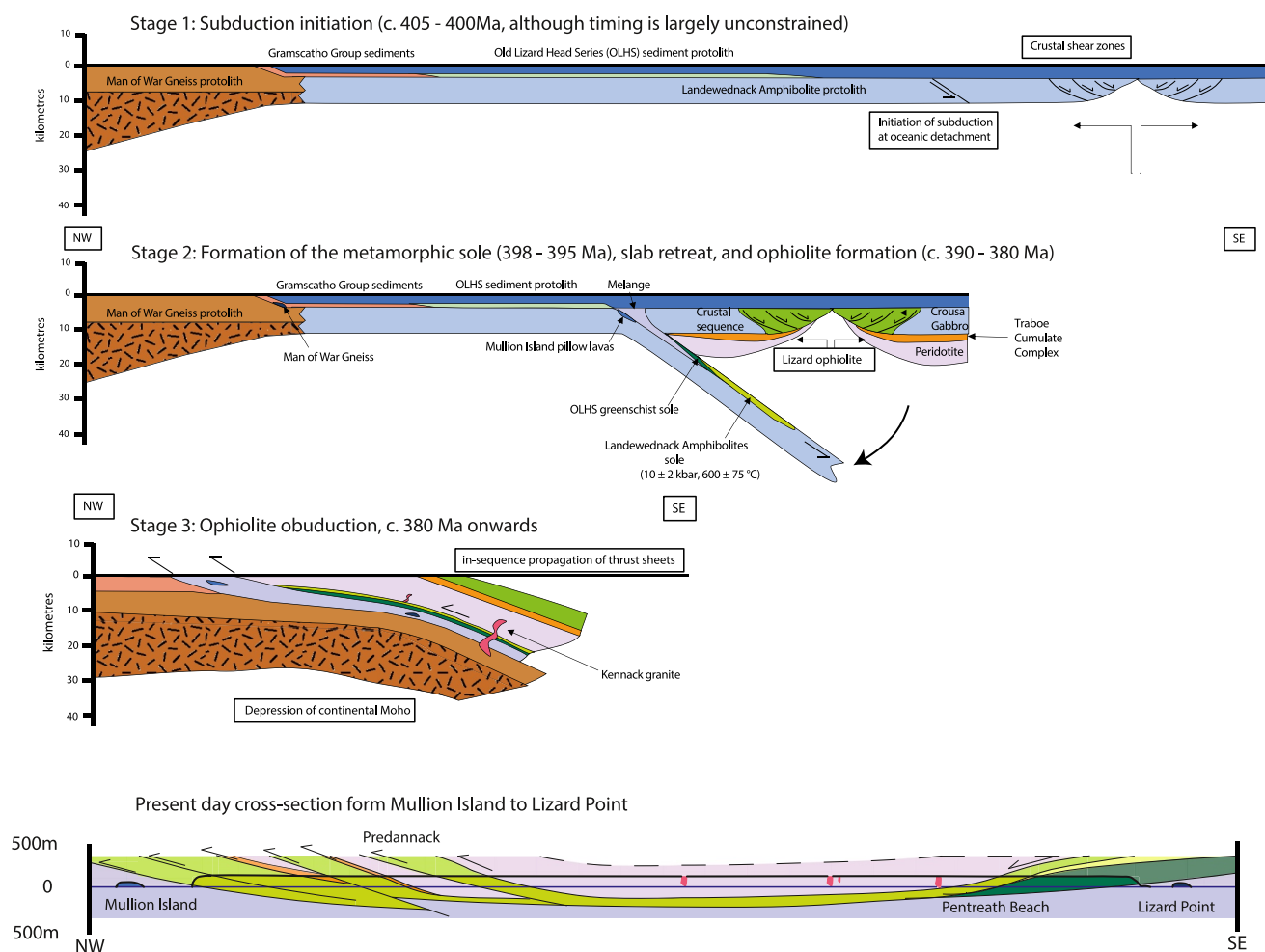


Figure 16. New tectonic model for the Lizard ophiolite.

interpretation of the Clark et al. (1998) “plagiogranite” and our new age of 395.08 ± 0.47 Ma). We interpret this as indicating that a south-east dipping oceanic subduction zone (in modern co-ordinates) was already established by this time (late Emsian, Lower Devonian) to the northwest of the Lizard ophiolite spreading ridge.

Our new 386.80 ± 0.52 Ma age of the Porthoustock plagiogranite is the first precise zircon U-Pb age to unequivocally date the formation age of the Lizard ophiolite. It clearly demonstrates that oceanic spreading was occurring during the Givetian (Middle Devonian) and therefore after the sole metamorphism event. This is supported by the previous geochronological data (Nutman et al., 2023) for the Traboe Cumulate Sequence, here interpreted as part of the crust-mantle boundary of the Lizard Ophiolite, which clusters around 390–380 Ma.

The current geochronological data does not permit an interpretation of the Kennack Gneiss. Around 380 Ma (+6/−10 Myr), the Landewednack Amphibolites and the Old Lizard Head Series cooled below the mica and hornblende Ar–Ar closure temperatures (Clark et al., 1998; Nutman et al., 2001), reflecting the exhumation of the sole. Mafic amphibolites at Kennack Sands cooled below the hornblende Ar–Ar closure temperature at c. 366 Ma (Sandeman et al., 1995). This likely represents cooling after final ophiolite emplacement.

10.3. Implications for the Variscan Orogeny

The Lizard ophiolite provides important constraints on the evolution of the Rheic-Renohercynian suture zone in the Variscan orogen. The correlative suture zone in Germany and Iberia records late Silurian to earliest Devonian closure of the Rheic Ocean followed, or accompanied by, the development of a narrow, short-lived, Renohercynian Ocean during the Early Devonian, that was closed by the end-Devonian during the onset of Variscan continent-continent collision (e.g., Arenas et al., 2014; Franke, 2000, 2024). Our new data are in permissive agreement with these models.

Subduction initiation and high P/T metamorphism of the Landwednack Amphibolites commenced prior to 395.08 ± 0.47 Ma (late Emsian) and the Renohercynian Lizard spreading center was active until 386.80 ± 0.52 Ma (early Givetian, Middle Devonian). If the 482 ± 12 – 478 ± 12 Ma volcanosedimentary zircons recorded in the Landwednack Amphibolites represent a magmatic protolith age (Nutman et al., 2023) then they must represent Rheic Oceanic crust that was subducted in the latest Silurian to Early Devonian. Alternatively, if these zircons were inherited, the Landwednack Amphibolites could represent earliest Devonian oceanic crust formed at the Renohercynian Lizard spreading center.

As a consequence, the Landwednack Amphibolites could record subduction associated with: (a) closure of a final tract of Rheic Ocean accompanied by Givetian (and earlier) formation of the SSZ Renohercynian Lizard spreading center (proposed in our model below), (b) late Silurian to early Devonian closure of the Rheic Ocean prior to Renohercynian rifting (e.g., Franke, 2000, 2024; Shail & Leveridge, 2009), or (c) Early Devonian subduction initiation within the Renohercynian Ocean. Distinguishing between these models is not presently possible but our study indicates Ordovician Rheic Ocean crust and Devonian Renohercynian Ocean crust may be preserved in the Lizard complex. As such there is similarity with the NW Iberia ophiolites (e.g., Arenas et al., 2014).

11. Conclusions

Our new model showing the tectonic evolution of the Lizard ophiolite and metamorphic sole rocks is presented in Figure 16 and discussed below.

11.1. Tectonics Prior to Ophiolite Formation

During the Cambrian, at 498 ± 11 Ma to 488 ± 11 Ma, continental magmatism on the margin of Avalonia (Laurussia) resulted in the formation of the Man of War Gneiss and felsic igneous bodies within the protolith of the Old Lizard Head Series. Subsequent continental rifting from at least 482 ± 12 Ma led to the creation of an oceanic spreading center at which oceanic crust with a MORB geochemistry formed. This timing is typical of the Avalonian margin (e.g., Žák et al., 2023). This oceanic crust was the protolith of the Landwednack Amphibolites, the epidote-amphibolites of Housel Bay, and the pillow lavas exposed on Mullion Island. It is possible that the banded epidote-amphibolites of Housel Bay represent the metamorphosed equivalents of the Mullion Island pillow basalts. The Mullion Island pillow basalts now form a large coherent block within the mélange unit (Roseland Breccia Formation) beneath the Lizard ophiolite. The protoliths of the Old Lizard Head Series are interpreted as siliceous and argillaceous sediments deposited in this marine setting with intervening tuffs or lava flows.

11.2. Subduction Initiation and Ophiolite Formation

During the early Devonian, a south-dipping, intraoceanic subduction zone was initiated within the Rheic Ocean, and the Landwednack amphibolites were formed by metamorphism of the upper crust of the downgoing slab between 398 and 395 Ma. The Landwednack amphibolites experienced partial melting at metamorphic conditions of up to 10 ± 2 kbar and $600 \pm 75^\circ\text{C}$. Our new U-Pb zircon ages suggest that incipient cooling after partial melting occurred at 395.08 ± 0.47 Ma (late Emsian).

Between 390 and 380 Ma (Lower and Middle Devonian), oceanic spreading formed the Traboe Cumulate Sequence and the Lizard ophiolite crust, including the Crousa Gabbro, plagiogranite dykes (386.80 ± 0.52 Ma; this study) and the Porthoustock sheeted dykes. Extensive ductile deformation was associated with low-angle normal faulting away from the ridge axis (e.g., Carrick Luz shear zone), and metasomatism is evidenced by fluid-rich shear zones preserved in the gabbro, inter-layering of amphibolite and peridotite in outcrops of the

Traboe Cumulate Sequence (e.g., Predannack). The 5 Myr age difference between the metamorphic sole and the ophiolite suggests a forced subduction initiation, with ophiolite spreading occurring as the result of slab rollback once the subduction became self-sustaining (e.g., Agard et al., 2020; Guilmette et al., 2018; Soret et al., 2022).

11.3. Ophiolite Obduction

Following metamorphism at c. 10 kbar, the metamorphic sole began its final stage of exhumation at around 380 Ma, as evidenced by the c. 380 Ma Ar–Ar mica cooling age of the Landewednack Amphibolites and the Old Lizard Head Series (Clark et al., 1998). During exhumation, the metamorphic sole was accreted to the base of the preserved ophiolite at conditions of 2–5 kbar and $721 \pm 44^\circ\text{C}$. The ongoing subduction of the slab beneath the ophiolite eventually brought continental crust into the subduction zone, as evidenced by the Kennack K-feldspar granites, which are interpreted to have formed from the burial and partial melting of continental sedimentary rocks (Sandeman et al., 1997). The Lizard ophiolite then likely followed the standard ophiolite obduction mechanism: The continental crust resisted subduction due to its low density relative to the mantle. A combination of slab break-off and the buoyancy of the continental crust resulted in the termination of subduction and “partial regurgitation” (Stern et al., 2012) of the subduction zone rocks.

As the Lizard ophiolite was emplaced onto the continent, it was thrust over the Roseland Breccia Formation mélange unit (including the Man of War Gneiss and the Mullion Island pillow basalts) and the Gramscatho Group foreland succession (Willment, 2019). The ophiolite was obducted from SSW to NNW as shown by the NNW–SSE aligned penetrative lineations throughout the peninsula. These lineations record high-temperature, plastic strain and are interpreted as showing the direction of ophiolite emplacement. There is also a spatial progression of ophiolite to metamorphic sole to mélange in a NW direction. Thus, the Lizard ophiolite has many similarities with better-constrained obducted ophiolites such as Oman (Rioux et al., 2012; Searle & Cox, 1999b; Searle & Malpas, 1980; Soret et al., 2022), where subduction initiation led to ophiolite formation, obduction, and final emplacement.

Data Availability Statement

The field data, electron-microprobe analysis data, the CA-ID-TIMS and laser ablation U–Pb data and XRF data used for structural analysis, geochronology, geochemistry and thermobarometry in the study are currently being archived at Oxford Research Archive for Data (ORA-Data). It can be accessed here: <https://doi.org/10.5287/bodleian:0zwDDM7Qm>.

Acknowledgments

This work has been supported by a grant from the NERC National Environmental Isotope Facility (no. 2394.0321), which the authors would like to gratefully acknowledge. T.C. Mackay-Champion would like to thank the Department of Earth Sciences at the University of Oxford for helping to cover the costs of fieldwork and sample analysis. M.P. Searle gratefully acknowledges a Leverhulme Emeritus Fellowship. The authors would also like to acknowledge Dave Waters (University of Oxford) for useful discussions, Stephan Buhre (JGU Mainz) for XRF analysis, Adrian Wood (British Geological Survey) for zircon processing, Jon Wells (previously at the University of Oxford) for thin sections, Phil Gopon (previously at the University of Oxford) for probe help, and Stephen Champion for assistance in the field.

References

- Agard, P., Prigent, C., Soret, M., Dubacq, B., Guillot, S., & Deldicque, D. (2020). Slabification: Mechanisms controlling subduction development and viscous coupling. *Earth-Science Reviews*, 208, 103259. <https://doi.org/10.1016/j.earscirev.2020.103259>
- Agard, P., Yamato, P., Soret, M., Prigent, C., Guillot, S., Plunder, A., et al. (2016). Plate interface rheological switches during subduction infancy: Control on slab penetration and metamorphic sole formation. *Earth and Planetary Science Letters*, 451, 208–220. <https://doi.org/10.1016/j.epsl.2016.06.054>
- Agrawal, S., Guevara, M., & Verma, S. P. (2008). Tectonic discrimination of basic and ultrabasic volcanic rocks through log-transformed ratios of immobile trace elements. *International Geology Review*, 50(12), 1057–1079. <https://doi.org/10.2747/0020-6814.50.12.1057>
- Alexander, A. C., Shail, R. K., & Leveridge, B. E. (2019). Late Paleozoic extensional reactivation of the Rheic–Rhenohercynian suture zone in SW England, the English Channel and western approaches. *Geological Society, London, Special Publications*, 470(1), 353–373. <https://doi.org/10.1144/SP470.19>
- Allerton, S., & Macleod, C. J. (1998). Fault-controlled magma transport through the mantle lithosphere at slow-spreading ridges. *Geological Society, London, Special Publications*, 148(1), 29–42. <https://doi.org/10.1144/GSL.SP.1998.148.01.03>
- Ambrose, T. K., Waters, D. J., Searle, M. P., Gopon, P., & Forshaw, J. B. (2021). Burial, accretion, and exhumation of the metamorphic sole of the Oman–UAE ophiolite. *Tectonics*, 40(4). <https://doi.org/10.1029/2020TC006392>
- Anonymous. (1972). Penrose field conference on ophiolites. *Geotimes*, 17, 24–25.
- Arenas, R., Fernández, R. D., Martínez, S. S., Gerdes, A., Fernández-Suárez, J., & Albert, R. (2014). Two-stage collision: Exploring the birth of Pangea in the Variscan terranes. *Gondwana Research*, 25(2), 756–763. <https://doi.org/10.1016/j.gr.2013.08.009>
- Beard, J. S., & Lofgren, G. E. (1991). Dehydration melting and water-saturated melting of basaltic and andesitic greenstones and amphibolites at 1, 3, and 6.9 kb. *Journal of Petrology*, 32(2), 365–401. <https://doi.org/10.1093/petrology/32.2.365>
- British Institutions Reflection Profiling Syndicate (BIRPS), & ETUDE DE LA CROÛTE CONTINENTALE ET OCÉANIQUE PAR RÉFLEXION ET RÉFRACTION SISMIQUE (ECORS). (1986). Deep seismic reflection profiling between England, France and Ireland. *Journal of the Geological Society*, 143(1), 45–52. <https://doi.org/10.1144/gsjgs.143.1.0045>
- Bromley, A. V. (1976). A new interpretation of the Lizard Complex, south Cornwall in the light of the ocean crust model. *Proceedings of the Journal of the Geological Society*, 132(1), 114. <https://doi.org/10.1144/gsjgs.132.1.0105>

- Clark, A. H., Sandeman, H. A. I., Nutman, A. P., Green, D. H., & Cook, A. (2003). Discussion on SHRIMP U–Pb zircon dating of the exhumation of the Lizard Peridotite and its emplacement over crustal rocks: Constraints for tectonic models. *Journal of the Geological Society*, 160(2), 331–335. <https://doi.org/10.1144/0016-764901-159>
- Clark, A. H., Scott, D. J., Sandeman, H. A., Bromley, A. V., & Farrar, E. (1998). Siegenian generation of the Lizard ophiolite: U–Pb zircon age data for plagiogranite, Porthkerris, Cornwall. *Journal of the Geological Society*, 155(4), 595–598. <https://doi.org/10.1144/gsjgs.155.4.0595>
- Coleman, R. G. (1971). Plate tectonic emplacement of upper mantle peridotites along continental edges. *Journal of Geophysical Research*, 76(5), 1212–1222. <https://doi.org/10.1029/JB076i005p01212>
- Cook, C. A. (1999). *The tectonic evolution of mantle rocks from the Lizard ophiolite complex, South-West England*. PhD. Durham University.
- Cook, C. A., Holdsworth, R. E., & Styles, M. T. (2002). The emplacement of peridotites and associated oceanic rocks from the Lizard Complex, southwest England. *Geological Magazine*, 139(1), 27–45. <https://doi.org/10.1017/S0016756801005933>
- Cook, C. A., Holdsworth, R. E., Styles, M. T., & Pearce, J. A. (2000). Pre-emplacement structural history recorded by mantle peridotites: An example from the Lizard Complex, SW England. *Journal of the Geological Society*, 157(5), 1049–1064. <https://doi.org/10.1144/jgs.157.5.1049>
- Cowan, R. J., Searle, M. P., & Waters, D. J. (2014). Structure of the metamorphic sole to the Oman Ophiolite, Sumeini Window and Wadi Tayyin: Implications for ophiolite obduction processes. *Geological Society Special Publication*, 392(1), 155–175. <https://doi.org/10.1144/SP392.8>
- Cox, J., Searle, M., & Pedersen, R. (1999). The petrogenesis of leucogranitic dykes intruding the northern Semail ophiolite, United Arab Emirates: Field relationships, geochemistry and Sr/Nd isotope systematics. *Contributions to Mineralogy and Petrology*, 137(3), 267–287. <https://doi.org/10.1007/s004100050550>
- Davies, G. R. (1984). Isotopic evolution of the Lizard Complex. *Journal of the Geological Society*, 141(1), 3–14. <https://doi.org/10.1144/gsjgs.141.1.0003>
- de Capitani, C., & Petrakakis, K. (2010). The computation of equilibrium assemblage diagrams with Theriak/Domino software. *American Mineralogist*, 95(7), 1006–1016. <https://doi.org/10.2138/am.2010.3354>
- Dilek, Y., & Furnes, H. (2014). Ophiolites and their origins. *Elements*, 10(2), 93–100. <https://doi.org/10.2113/gselements.10.2.93>
- Duretz, T., Agard, P., Yamato, P., Ducassou, C., Burov, E. B., & Gerya, T. V. (2016). Thermo-mechanical modeling of the obduction process based on the Oman ophiolite case. *Gondwana Research*, 32, 1–10. <https://doi.org/10.1016/j.gr.2015.02.002>
- Eckelmann, K., Nesbor, H. D., Königshof, P., Linnemann, U., Hofmann, M., Lange, J. M., & Sagawe, A. (2014). Plate interactions of Laurussia and Gondwana during the formation of Pangaea—Constraints from U–Pb LA-SF-ICP-MS detrital zircon ages of Devonian and Early Carboniferous siliciclastics of the Rhenohercynian zone, Central European Variscides. *Gondwana Research*, 25(4), 1484–1500. <https://doi.org/10.1016/j.gr.2013.05.018>
- Flett, J. S., & Hill, J. B. (1946). *Geology of the Lizard and Meneage: (explanation of sheet 359)* (Vol. 359). HM Stationery Office.
- Floyd, P. A. (1995). Igneous activity. In R. D. Dallmeyer, W. Franke, & K. Weber (Eds.), *Pre-Permian geology of central and eastern Europe* (pp. 59–81). Springer Berlin Heidelberg. <https://doi.org/10.1007/978-3-642-77518-5>
- Forshaw, J. B., Waters, D. J., Pattison, D. R. M., Palin, R. M., & Gopon, P. (2019). A comparison of observed and thermodynamically predicted phase equilibria and mineral compositions in mafic granulites. *Journal of Metamorphic Geology*, 37(2), 153–179. <https://doi.org/10.1111/jmg.12454>
- Franke, W. (2000). The mid-European segment of the Variscides: Tectonostratigraphic units, terrane boundaries and plate tectonic evolution. *Geological Society, London, Special Publications*, 179(1), 35–61. <https://doi.org/10.1144/GSL.SP.2000.179.01.05>
- Franke, W. (2024). The Rheic riddle: Ocean closed, but no orogen. *Geological Society, London, Special Publications*, 542(1), SP542–2022. <https://doi.org/10.1144/SP542-2022-354>
- Franke, W., Cocks, L. R. M., & Torsvik, T. H. (2017). The Palaeozoic Variscan oceans revisited. *Gondwana Research*, 48, 257–284. <https://doi.org/10.1016/j.gr.2017.03.005>
- Gale, A., Dalton, C. A., Langmuir, C. H., Su, Y., & Schilling, J. (2013). The mean composition of ocean ridge basalts. *Geochemistry, Geophysics, Geosystems*, 14(3), 489–518. <https://doi.org/10.1029/2012GC004334>
- Gibbons, W., & Thompson, L. (1991). Ophiolitic mylonites in the Lizard Complex: Ductile extension in the lower oceanic crust. *Geology*, 19(10), 1009–1012. [https://doi.org/10.1130/0091-7613\(1991\)019<1009:OMITLC>2.3.CO;2](https://doi.org/10.1130/0091-7613(1991)019<1009:OMITLC>2.3.CO;2)
- Green, D. H. (1964a). The metamorphic aureole of the peridotite at the Lizard, Cornwall. *The Journal of Geology*, 72(5), 543–563. <https://doi.org/10.1086/627013>
- Green, D. H. (1964b). The petrogenesis of the high-temperature peridotite intrusion in the Lizard area, Cornwall. *Journal of Petrology*, 5(1), 134–188. <https://doi.org/10.1093/petrology/5.1.134>
- Green, E. C. R., White, R. W., Diener, J. F. A., Powell, R., Holland, T. J. B., & Palin, R. M. (2016). Activity–composition relations for the calculation of partial melting equilibria in metabasic rocks. *Journal of Metamorphic Geology*, 34(9), 845–869. <https://doi.org/10.1111/jmg.12211>
- Guilmette, C., Smit, M. A., van Hinsbergen, D. J. J., Gürer, D., Corfu, F., Charette, B., et al. (2018). Forced subduction initiation recorded in the sole and crust of the Semail Ophiolite of Oman. *Nature Geoscience*, 11(9), 688–695. <https://doi.org/10.1038/s41561-018-0209-2>
- Gurnis, M., Hall, C., & Lavier, L. (2004). Evolving force balance during incipient subduction. *Geochemistry, Geophysics, Geosystems*, 5(7), Q07001. <https://doi.org/10.1029/2003GC000681>
- Hall, C. E., Gurnis, M., Sdrolias, M., Lavier, L. L., & Müller, R. (2003). Catastrophic initiation of subduction following forced convergence across fracture zones. *Earth and Planetary Science Letters*, 212(1–2), 15–30. [https://doi.org/10.1016/S0012-821X\(03\)00242-5](https://doi.org/10.1016/S0012-821X(03)00242-5)
- Harvey, M. J., Stewart, S. A., Wilkinson, J. J., Ruffell, A. H., & Shail, R. K. (1994). Tectonic evolution of the Plymouth Bay Basin. *Proceedings of the Ussher Society*, 8(3), 271–278.
- Hernández-Urbe, D., & Palin, R. M. (2019). A revised petrological model for subducted oceanic crust: Insights from phase equilibrium modelling. *Journal of Metamorphic Geology*, 37(6), 745–768. <https://doi.org/10.1111/jmg.12483>
- Holder, M. T., & Leveridge, B. E. (1986). A model for the tectonic evolution of South Cornwall. *Journal of the Geological Society*, 143(1), 125–134. <https://doi.org/10.1144/gsjgs.143.1.0125>
- Holland, T., & Blundy, J. (1994). Non-ideal interactions in calcic amphiboles and their bearing on amphibole-plagioclase thermometry. *Contributions to Mineralogy and Petrology*, 116(4), 433–447. <https://doi.org/10.1007/BF00310910>
- Holland, T. J. B., & Powell, R. (2011). An improved and extended internally consistent thermodynamic dataset for phases of petrological interest, involving a new equation of state for solids. *Journal of Metamorphic Geology*, 29(3), 333–383. <https://doi.org/10.1111/j.1525-1314.2010.00923.x>
- Hora, J. M., Kronz, A., Möller-McNett, S., & Wörner, G. (2013). An Excel-based tool for evaluating and visualizing geothermobarometry data. *Computers & Geosciences*, 56, 178–185. <https://doi.org/10.1016/j.cageo.2013.02.008>
- Ishizuka, O., Taylor, R. N., Yuasa, M., & Ohara, Y. (2011). Making and breaking an island arc: A new perspective from the Oligocene Kyushu–Palau arc, Philippine Sea. *Geochemistry, Geophysics, Geosystems*, 12(5), Q05005. <https://doi.org/10.1029/2010gc003440>

- Jamieson, R. A. (1980). Formation of metamorphic aureoles beneath ophiolites—Evidence from the St. Anthony Complex, Newfoundland. *Geology*, 8(3), 150–154. [https://doi.org/10.1130/0091-7613\(1980\)8<150:FORABO>2.0.CO;2](https://doi.org/10.1130/0091-7613(1980)8<150:FORABO>2.0.CO;2)
- Jones, K. A. (1994). The most southerly point thrust—An example of ductile thrusting in the Lizard Complex, South-West Cornwall. *Geoscience in South-West England*, 8(3), 254–261.
- Jones, K. A. (1997). Deformation and emplacement of the Lizard Ophiolite Complex, SW England, based on evidence from the Basal Unit. *Journal of the Geological Society*, 154(5), 871–885. <https://doi.org/10.1144/gsjgs.154.5.0871>
- Keenan, T. E., Encarnación, J., Buchwaldt, R., Fernandez, D., Mattinson, J., Rasoazanamparany, C., & Luetkemeyer, P. B. (2016). Rapid conversion of an oceanic spreading center to a subduction zone inferred from high-precision geochronology. *Proceedings of the National Academy of Sciences of the United States of America*, 113(47), 1699999113. <https://doi.org/10.1073/pnas.1609999113>
- Kirby, G. A. (1979). The Lizard Complex as an ophiolite. *Nature*, 282(5734), 58–61. <https://doi.org/10.1038/282058a0>
- Klempner, S., & Hobbs, R. (1992). The BIRPS atlas: Deep seismic reflection profiles around the British Isles, the BIRPS atlas: Deep seismic reflection profiles around the British Isles. Retrieved from <https://www.scopus.com/inward/record.uri?eid=2-s2.0-85040955974&partnerID=40&md5=f370f35b5a7c886e483164045c89764>
- Leake, B. E., Woolley, A. R., Arps, C. E. S., Birch, W. D., Gilbert, M. C., Grice, J. D., et al. (1997). Nomenclature of amphiboles; report of the subcommittee on amphiboles of the international mineralogical association commission on new minerals and mineral names. *Mineralogical Magazine*, 61(405), 295–310. <https://doi.org/10.1180/minmag.1997.061.405.13>
- Leake, R. C., & Styles, M. T. (1984). Borehole sections through the Traboe hornblende schists, a cumulate complex overlying the Lizard peridotite. *Journal of the Geological Society*, 141(1), 41–52. <https://doi.org/10.1144/gsjgs.141.1.0041>
- le Gall, B. (1990). Evidence of an imbricate crustal thrust belt in the southern British Variscides: Contributions of southwestern approaches traverse (SWAT) deep seismic reflection profiling recorded through the English Channel and the Celtic Sea. *Tectonics*, 9(2), 283–302. <https://doi.org/10.1029/TC009i002p00283>
- Leveridge, B. E., & Shail, R. K. (2011). The Gramscatho Basin, South Cornwall, UK: Devonian active margin successions. *Proceedings of the Geologists' Association*, 122(4), 568–615. <https://doi.org/10.1016/j.pgeola.2011.03.004>
- Malpas, J., & Langdon, G. S. (1987). The Kennack Gneisses of the Lizard Complex, Cornwall, England: Partial melts produced during ophiolite emplacement. *Canadian Journal of Earth Sciences*, 24(10), 1966–1974. <https://doi.org/10.1139/e87-187>
- Mann, H. B., & Whitney, D. R. (1947). On a test of whether one of two random variables is stochastically larger than the other. *The Annals of Mathematical Statistics*, 18(1), 50–60. <https://doi.org/10.1214/aoms/1177730491>
- Murphy, J. B., Gutierrez-Alonso, G., Nance, R. D., Fernandez-Suarez, J., Keppie, J. D., Quesada, C., et al. (2006). Origin of the Rheic Ocean: Rifting along a Neoproterozoic suture? *Geology*, 34(5), 325. <https://doi.org/10.1130/G22068.1>
- Nance, R. D., & Linnemann, U. (2008). The Rheic Ocean: Origin, evolution, and significance. *Geological Society of America Today*, 18(12), 4–12. <https://doi.org/10.1130/GSATG24A.1>
- Nutman, A. P., Bennett, V. C., Green, D. H., & Friend, C. R. L. (2023). Evolution of the Palaeozoic mafic-ultramafic Lizard Complex (SW England) from zircon and baddeleyite U-Pb-Hf isotopic constraints: New thoughts on the convergence of Avalonia and Armorica. *Lithos*, 452–453, 107227. <https://doi.org/10.1016/j.lithos.2023.107227>
- Nutman, A. P., Green, D. H., Cook, C. A., Styles, M. T., & Holdsworth, R. E. (2001). SHRIMP U–Pb zircon dating of the exhumation of the Lizard Peridotite and its emplacement over crustal rocks: Constraints for tectonic models. *Journal of the Geological Society*, 158(5), 809–820. <https://doi.org/10.1144/jgs.158.5.809>
- Palin, R. M., Weller, O. M., Waters, D. J., & Dyck, B. (2016). Quantifying geological uncertainty in metamorphic phase equilibria modelling: A Monte Carlo assessment and implications for tectonic interpretations. *Geoscience Frontiers*, 7(4), 591–607. <https://doi.org/10.1016/j.gsf.2015.08.005>
- Pearce, J. A. (2014). Immobile element fingerprinting of ophiolites. *Elements*, 10(2), 101–108. <https://doi.org/10.2113/gselements.10.2.101>
- Pearce, J. A., Alabaster, T., Shelton, A. W., & Searle, M. P. (1981). The Oman ophiolite as a Cretaceous arc-basin complex: Evidence and implications. *Philosophical Transactions of the Royal Society of London—Series A: Mathematical and Physical Sciences*, 300(1454), 299–317. <https://doi.org/10.1098/rsta.1981.0066>
- Pearce, J. A., Harris, N. B. W., & Tindle, A. G. (1984). Trace element discrimination diagrams for the tectonic interpretation of granitic rocks. *Journal of Petrology*, 25(4), 956–983. <https://doi.org/10.1093/petrology/25.4.956>
- Penniston-Dorland, S. C., Kohn, M. J., & Manning, C. E. (2015). The global range of subduction zone thermal structures from exhumed blueschists and eclogites: Rocks are hotter than models. *Earth and Planetary Science Letters*, 428, 243–254. <https://doi.org/10.1016/j.epsl.2015.07.031>
- Reynolds, P., Holford, S., Schofield, N., & Ross, A. (2017). Three-dimensional seismic imaging of ancient submarine lava flows: An example from the southern Australian margin. *Geochemistry, Geophysics, Geosystems*, 18(11), 3840–3853. <https://doi.org/10.1002/2017GC007178>
- Rioux, M., Benoit, M., Amri, I., Ceuleneer, G., Garber, J. M., Searle, M., & Leal, K. (2021). The origin of felsic intrusions within the mantle section of the Samail Ophiolite: Geochemical evidence for three distinct mixing and fractionation trends. *Journal of Geophysical Research: Solid Earth*, 126(5), e2020JB020760. <https://doi.org/10.1029/2020JB020760>
- Rioux, M., Bowring, S., Kelemen, P., Gordon, S., Dudás, F., & Miller, R. (2012). Rapid crustal accretion and magma assimilation in the Oman-U. A.E. ophiolite: High precision U-Pb zircon geochronology of the gabbroic crust. *Journal of Geophysical Research*, 117(7), B07201. <https://doi.org/10.1029/2012JB009273>
- Roberts, N. M. W., Parrish, R. R., Horstwood, M. S. A., & Brewer, T. S. (2011). The 1.23 Ga Fjellhovdane rhyolite, Grøsså-Totak; a new age within the Telemark supracrustals, southern Norway. *Norsk Geologisk Tidsskrift*, 91(4), 239–246. <https://www.scopus.com/inward/record.uri?eid=2-s2.0-84863579514&partnerID=40&md5=0a1328304069a6c713e35c75031ec333>
- Roberts, S., Andrews, J., Bull, J., & Sanderson, D. (1993). Slow-spreading ridge-axis tectonics: Evidence from the Lizard Complex, UK. *Earth and Planetary Science Letters*, 116(1–4), 101–112. [https://doi.org/10.1016/0012-821X\(93\)90047-D](https://doi.org/10.1016/0012-821X(93)90047-D)
- Rollinson, H. (2014). Plagiogranites from the mantle section of the Oman Ophiolite: Models for early crustal evolution. *Geological Society, London, Special Publications*, 392(1), 247–261. <https://doi.org/10.1144/SP392.13>
- Rollinson, H., & Pease, V. (2021). *Using geochemical data* (Vol. 62). Cambridge University Press. <https://doi.org/10.1017/9781108777834>
- Saccani, E. (2015). A new method of discriminating different types of post-Archean ophiolitic basalts and their tectonic significance using Th-Nb and Ce-Dy-Yb systematics. *Geoscience Frontiers*, 6(4), 481–501. <https://doi.org/10.1016/j.gsf.2014.03.006>
- Sandeman, H. A., Chen, Y., Clark, A. H., & Farrar, E. (1995). Constraints on the P–T conditions and age of emplacement of the Lizard ophiolite, Cornwall: Amphibole–plagioclase thermobarometry and ⁴⁰Ar/³⁹Ar geochronology of basal amphibolites. *Canadian Journal of Earth Sciences*, 32(3), 261–272. <https://doi.org/10.1139/e95-021>

- Sandeman, H. A., Clark, A. H., Styles, M. T., Scott, D. J., Malpas, J. G., & Farrar, E. (1997). Geochemistry and U-Pb and ^{40}Ar - ^{39}Ar geochronology of The Man of War Gneiss, Lizard Complex, SW England: Pre-Hercynian arc-type crust with a Sudeten-Iberian connection. *Journal of the Geological Society*, 154(3), 403–417. <https://doi.org/10.1144/gsjgs.154.3.0403>
- Sandeman, H. A. I. (1988). *A field, petrographical and geochemical investigation. Of the Kennack Gneiss, Lizard Peninsula, southwest England*. Masters. Memorial University of Newfoundland.
- Sandeman, H. A. I., Clark, A. H., Scott, D. J., & Malpas, J. G. (2000). The Kennack Gneiss of the Lizard Peninsula, Cornwall, SW England: Commingling and mixing of mafic and felsic magmas accompanying Givetian continental incorporation of the Lizard ophiolite. *Journal of the Geological Society*, 157(6), 1227–1242. <https://doi.org/10.1144/jgs.157.6.1227>
- Sawyer, E. W. (2008). *Atlas of migmatites* (Vol. 9). Canadian Science Publishing. <https://doi.org/10.1139/9780660197876>
- Schumacher, J. C. (2007). Metamorphic amphiboles: Composition and coexistence. *Reviews in Mineralogy and Geochemistry*, 67(1), 359–416. <https://doi.org/10.2138/rmg.2007.67.10>
- Searle, M., & Cox, J. (1999a). Tectonic setting, origin, and obduction of the Oman ophiolite. *Bulletin of the Geological Society of America*, 111(1), 104–122. [https://doi.org/10.1130/0016-7606\(1999\)111<0104:TSOAO>2.3.CO;2](https://doi.org/10.1130/0016-7606(1999)111<0104:TSOAO>2.3.CO;2)
- Searle, M., & Cox, J. (1999b). Tectonic setting, origin, and obduction of the Oman ophiolite. *Bulletin of the Geological Society of America*, 111(1), 104–122. [https://doi.org/10.1130/0016-7606\(1999\)111<0104:TSOAO>2.3.CO;2](https://doi.org/10.1130/0016-7606(1999)111<0104:TSOAO>2.3.CO;2)
- Searle, M. P., & Cox, J. (2002). Subduction zone metamorphism during formation and emplacement of the Semail ophiolite in the Oman Mountains. *Geological Magazine*, 139(3), 241–255. <https://doi.org/10.1017/S0016756802006532>
- Searle, M. P., & Malpas, J. (1980). Structure and metamorphism of rocks beneath the Semail ophiolite of Oman and their significance in ophiolite obduction. *Earth Sciences*, 71(4), 247–262. <https://doi.org/10.1017/S0263593300013614>
- Searle, M. P., & Malpas, J. (1982). Petrochemistry and origin of sub-ophiolitic metamorphic and related rocks in the Oman Mountains. *Journal of the Geological Society*, 139(3), 235–248. <https://doi.org/10.1144/gsjgs.139.3.0235>
- Shail, R. K., & Leveridge, B. E. (2009). The Rheohercynian passive margin of SW England: Development, inversion and extensional reactivation. *Comptes Rendus Geoscience*, 341(2–3), 140–155. <https://doi.org/10.1016/j.crte.2008.11.002>
- Soret, M., Agard, P., Dubacq, B., Plunder, A., & Yamato, P. (2017). Petrological evidence for stepwise accretion of metamorphic soles during subduction infancy (Semail ophiolite, Oman and UAE). *Journal of Metamorphic Geology*, 35(9), 1051–1080. <https://doi.org/10.1111/jmg.12267>
- Soret, M., Bonnet, G., Agard, P., Larson, K., Cottle, J., Dubacq, B., et al. (2022). Timescales of subduction initiation and evolution of subduction thermal regimes. *Earth and Planetary Science Letters*, 584, 117521. <https://doi.org/10.1016/j.epsl.2022.117521>
- Stern, R. J. (2004). Subduction initiation: Spontaneous and induced. *Earth and Planetary Science Letters*, 226(3–4), 275–292. <https://doi.org/10.1016/j.epsl.2004.08.007>
- Stern, R. J., Reagan, M., Ishizuka, O., Ohara, Y., & Whattam, S. (2012). To understand subduction initiation, study forearc crust: To understand forearc crust, study ophiolites. *Lithosphere*, 4(6), 469–483. <https://doi.org/10.1130/L183.1>
- Strong, D. F., Stevens, R. K., Malpas, J., & Badham, J. P. N. (1975). A new tale for the Lizard. *Proceedings of the Ussher Society*, 3(2), 252.
- Styles, M. T., & Kirby, G. A. (1980). New investigations of the Lizard Complex, Cornwall, England and a discussion of an ophiolite model. *Ophiolites*, 517–526.
- Styles, M. T., & Rundle, C. C. (1984). The Rb-Sr isochron age of the Kennack gneiss and its bearing on the age of the Lizard Complex, Cornwall. *Journal of the Geological Society*, 141(1), 15–19. <https://doi.org/10.1144/gsjgs.141.1.0015>
- Tapster, S., Condon, D., Naden, J., Noble, S., Petterson, M., Roberts, N., et al. (2016). Rapid thermal rejuvenation of high-crystallinity magma linked to porphyry copper deposit formation; evidence from the Koloula Porphyry Prospect, Solomon Islands. *Earth and Planetary Science Letters*, 442, 206–217. <https://doi.org/10.1016/j.epsl.2016.02.046>
- Teall, J. J. H. (1886). I.—The metamorphosis of the Lizard Gabbros. *Geological Magazine*, 3(11), 481–489. <https://doi.org/10.1017/S0016756800466732>
- van Hinsbergen, D. J. J., Peters, K., Maffione, M., Spakman, W., Guilmette, C., Thieulot, C., et al. (2015). Dynamics of intraoceanic subduction initiation: 2. Suprasubduction zone ophiolite formation and metamorphic sole exhumation in context of absolute plate motions. *Geochemistry, Geophysics, Geosystems*, 16(6), 1771–1785. <https://doi.org/10.1002/2015GC005745>
- Varga, R. J., & Moores, E. M. (1985). Spreading structure of the Troodos ophiolite, Cyprus. *Geology*, 13(12), 846–850. [https://doi.org/10.1130/0091-7613\(1985\)13<846:SSOTTO>2.0.CO;2](https://doi.org/10.1130/0091-7613(1985)13<846:SSOTTO>2.0.CO;2)
- Wakabayashi, J., & Dilek, Y. (2000). Spatial and temporal relationships between ophiolites and their metamorphic soles: A test of models of forearc ophiolite genesis. In *Ophiolites and oceanic crust: New insights from field studies and the ocean drilling program*. Geological Society of America. <https://doi.org/10.1130/0-8137-2349-3.53>
- White, J. D. L., McPhie, J., & Soule, S. A. (2015). Chapter 19—Submarine lavas and hyaloclastite. In H. Sigurdsson (Ed.), *The encyclopedia of volcanoes* (2nd ed.) (pp. 363–375). Academic Press. <https://doi.org/10.1016/B978-0-12-385938-9.00019-5>
- Williams, H., & Smyth, W. R. (1973). Metamorphic aureoles beneath ophiolite suites and alpine peridotites; tectonic implications with west Newfoundland examples. *American Journal of Science*, 273(7), 594–621. <https://doi.org/10.2475/ajs.273.7.594>
- Willment, G. (2019). *Structures beneath the Lizard ophiolite, Cornwall, southwest England*. Masters. University of Oxford.
- Žák, J., Jiří Sláma, J., Reza Syahputra, J., & Damian Nance, R. (2023). Dynamics of Cambro–Ordovician rifting of the northern margin of Gondwana as revealed by the timing of subsidence and magmatism in rift-related basins. *International Geology Review*, 65(19), 3004–3027. <https://doi.org/10.1080/00206814.2023.2172619>

References From the Supporting Information

- Condon, D. J., Schoene, B., McLean, N. M., Bowring, S. A., & Parrish, R. R. (2015). Metrology and traceability of U–Pb isotope dilution geochronology (EARTHTIME Tracer Calibration Part I). *Geochimica et Cosmochimica Acta*, 164, 464–480. <https://doi.org/10.1016/j.gca.2015.05.026>
- Horstwood, M. S. A., Košler, J., Gehrels, G., Jackson, S. E., McLean, N. M., Paton, C., et al. (2016). Community-derived standards for LA-ICP-MS-U-(Th)-Pb geochronology—Uncertainty propagation, age interpretation and data reporting. *Geostandards and Geoanalytical Research*, 40(3), 311–332. <https://doi.org/10.1111/j.1751-908X.2016.00379.x>
- McLean, N. M., Condon, D. J., Schoene, B., & Bowring, S. A. (2015). Evaluating uncertainties in the calibration of isotopic reference materials and multi-element isotopic tracers (EARTHTIME Tracer Calibration Part II). *Geochimica et Cosmochimica Acta*, 164, 481–501. <https://doi.org/10.1016/j.gca.2015.02.040>

- Paton, C., Hellstrom, J., Paul, B., Woodhead, J., & Hergt, J. (2011). Iolite: Freeware for the visualisation and processing of mass spectrometric data. *Journal of Analytical Atomic Spectrometry*, 26(12), 2508. <https://doi.org/10.1039/c1ja10172b>
- Tapster, S., Condon, D. J., Naden, J., Noble, S. R., Petterson, M. G., Roberts, N. M. W., et al. (2016). Rapid thermal rejuvenation of high-crystallinity magma linked to porphyry copper deposit formation; evidence from the Koloula Porphyry Prospect, Solomon Islands. *Earth and Planetary Science Letters*, 442, 206–217. <https://doi.org/10.1016/j.epsl.2016.02.046>
- Vermeesch, P. (2018). IsoplotR: A free and open toolbox for geochronology. *Geoscience Frontiers*, 9(5), 1479–1493. <https://doi.org/10.1016/j.gsf.2018.04.001>
- Wiedenbeck, M., Allé, P., Corfu, F., Griffin, W. L., Meier, M., Oberli, F., et al. (1995). Three natural zircon standard for U-Th-Pb, Lu-Hf, trace element and REE analyses. *Geostandards and Geoanalytical Research*, 19(1), 1–23. <https://doi.org/10.1111/j.1751-908X.1995.tb00147.x>